Development and refinement of regional sediment mobility models: Implications for coastal evolution, preservation of archaeological potential, and commercial development

Adam Carrizales

May 20, 2010

Abstract

Development of high-resolution hydrodynamic and sediment transport models for the Goodwin Sands and Outer Thames Estuary (UK) using a newly-obtained bathymetric dataset allows for accurate qualitative prediction of net sediment transport and bed level changes on a regional-scale. Iterative calibration of the hydrodynamic models used shows that use of a higher Manning's number friction coefficient than calculated based on physical conditions is required to compensate for bedforms not accurately resolvable by the bathymetric resolution. Application of the calibrated hydrodynamics models to drive sediment transport models allows for the testing of sandbank mobility in the Goodwin Sands and Outer Thames Estuary with favourable agreement between available swath bathymetry and previous studies of mobility. The overall model outputs conform to the accuracy standards laid out by the Environment Agency and as such the sediment mobility models developed in this project can be used for underwater resource and heritage management.

Contents

List of Figures

1 Introduction

The use of large-scale sediment transport models plays a key role in developing a better understanding of the underwater physical processes which govern sediment mobility, erosion and accumulation; and the effects of this movement. The development of viable sediment transport and hydrodynamic models covering a regional-scale is crucial for the effective management of underwater resources and heritage, as well as examining historical coastal evolution. The predictions obtained from sediment transport models are useful to a wide variety of end-users such as the offshore construction and aggregate extraction industries, as well as being used by heritage managers to assess areas of marine archaeological potential (AMAPs). These uses are derived from the ability of sediment transport models to predict areas of erosion and accumulation, and thus be able to evaluate overall bedform stability for resource and risk management.

This report will describe advances made in the development of two regional-scale sediment mobility models pertaining to the areas of **(1)** the Goodwin Sands, Kent and **(2)** the Outer Thames Estuary, Southern North Sea. The terms in which the results of these models are examined and discussed are as follows: **(i)** Overall accuracy of hydrodynamic model i.e. calibration **(ii)** Comparison of predicted sediment transport with geophysical datasets **(iii)** assessment of sandbank mobility in terms of present and historical changes **(iv)** assessment of the preservation potential for AMAPs.

1.1 Background

The two study areas are located at the juncture of two major water bodies, the English Channel and Southern North Sea. This results in a hydrodynamic regime that is tidally dominated, with water depths ranging between 0 and -75m MSL within the study area. The currents in the region are dominated by the tidal flow running coast-parallel in the Outer Thames Estuary (NNE/SSW) and north-south towards the Dover Strait, with the primary forcing provided by the semi-diurnal lunar (M2) constituent (Anthony, 2002; REC, 2009). The flood cycle flow is to the south/south-west and ebb cycle to the north/north-east with peak current velocities of 1.36 ms^{-1} and 1.41 ms^{-1} respectively (REC, 2009).

1.1.1 Goodwin Sands

The Goodwin Sands are a set of two large sandbanks, the "North Goodwins" and "South Goodwins" located 4-8 km from the East Kent Coast, covering an area of 90 km^2. The sandbanks are extremely shallow with crests at +3 metres MSL, with large portions of the banks drying out at low water (Fig. 1). It has been suggested that the sandbanks themselves are composed of approximately 25 metres of unconsolidated sands deposited on a chalk substratum which is commonly outcrops along the East Kent Coast. This large deposit suggests an area dominated by accumulation by tidal flow. Mobility of the Goodwin Sands has been studied in the past, most notably by Cloet (1954) who suggested the sandbanks rotate anti-clockwise slowly on a time-scale measured in decades. This corresponds to a movement of the North Goodwins to the north and west, and the eastern movement of the South Goodwins. Provided the hydrodynamic model is suitably calibrated to ensure its accuracy, the outputs of the sediment transport model can be used to test the hypothesis put forward by Cloet (1954) and provide evidence of sandbank mobility in the Goodwins.

Interest in the Goodwin Sands stems from their propensity for causing shipwrecks. Due to their shallow nature and proximity to major shipping routes, both at present and in the past, as many as 2000 ships are believed to have been wrecked on the Goodwins. This includes 5 UK Designated Wreck Sites (Restoration, Stirling Castle, Northumberland, Rooswijk, Admiral Gardner).

Much effort has been spent trying to gain a better understanding of the complex hydrodynamic regimes governing sediment dynamics of maritime archaeological sites in recent years. Past work includes models developed from single- and multi-site studies as well as in-situ measurements and calibrated tank experiments. While these studies are an excellent way of looking at individual wreck sites, they are very time consuming and expensive to carry out, especially when considering multiple sites. Given that on a national scale, there are hundreds to thousands of possible wreck sits, it quickly becomes inefficient to examine them in this light.

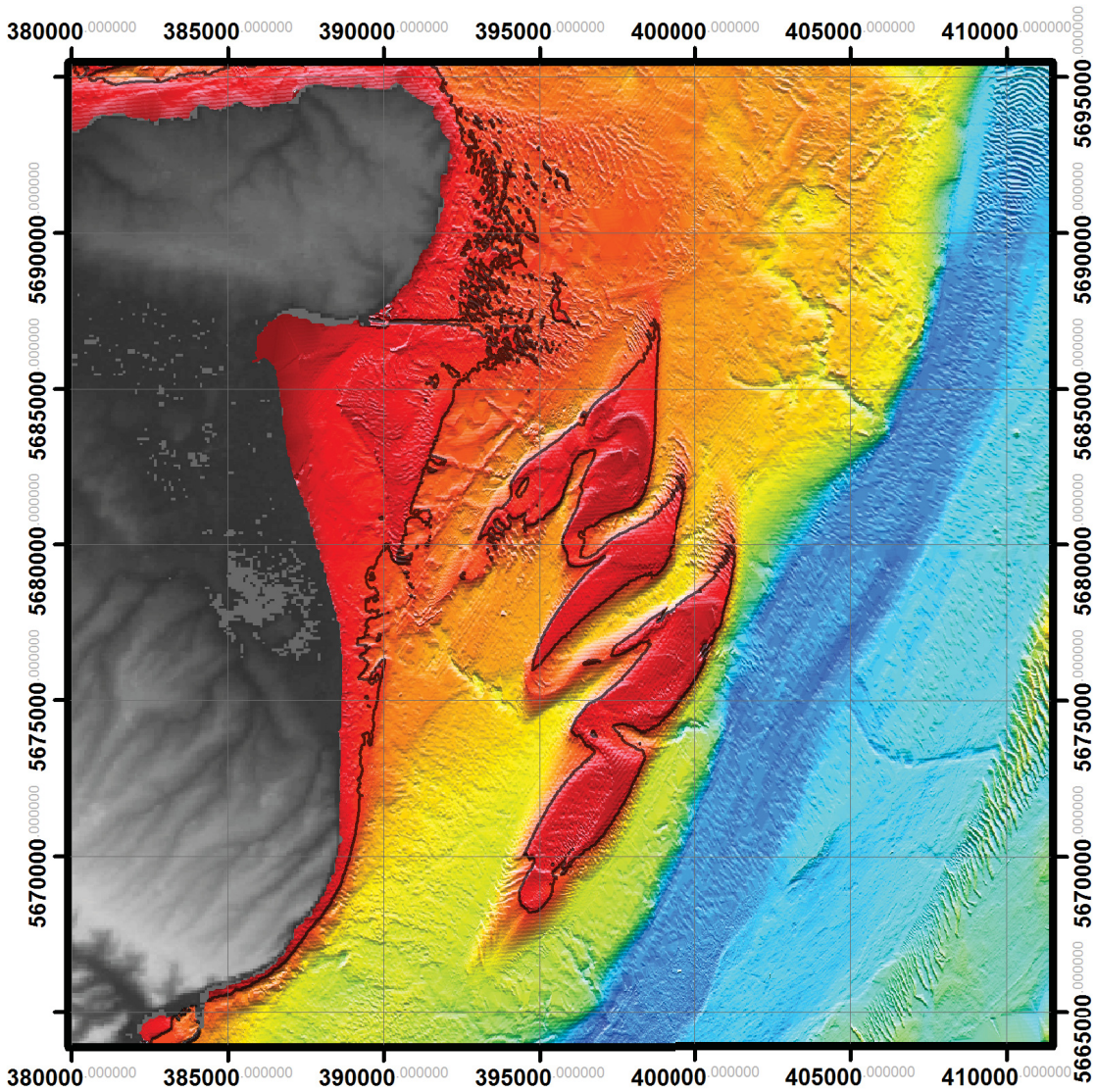

Figure 1 – Bathymetry of the Goodwin Sands and surrounding region, with 10 m depth contour (black). Depths in the region range from 0 m (red) to -75 m (blue) MSL. The sandbanks lie upon the chalk platform at c. -20 m depth.

Previous studies have also shown that laboratory or 'in-situ' methods applied to individual wreck sites may not be entirely accurate as there is a shortfall in the amount of information gathered around these sites regarding the large-scale coastal processes that may affect the region. Given the possibility of spatial and temporal variation in coastal environments, it becomes clear that a method for quantifying these processes in terms of both hydrodynamics and sediment dynamics on a large-scale is key to developing a way to quickly and efficiently identify AMAPs and begin taking steps to ensure their preservation.

1.1.2 Outer Thames Estuary (OTE)

The Outer Thames Estuary (OTE) lies offshore of south-east England on the margins of the Southern North Sea (SNS). As the OTE encompasses a much larger region than the Goodwin Sands (5400 km^2), for the purposes of this study it has been sub-divided into two morphological zones (Figures 2, 3 & 5):

- The Western Zone
- The Eastern Zone

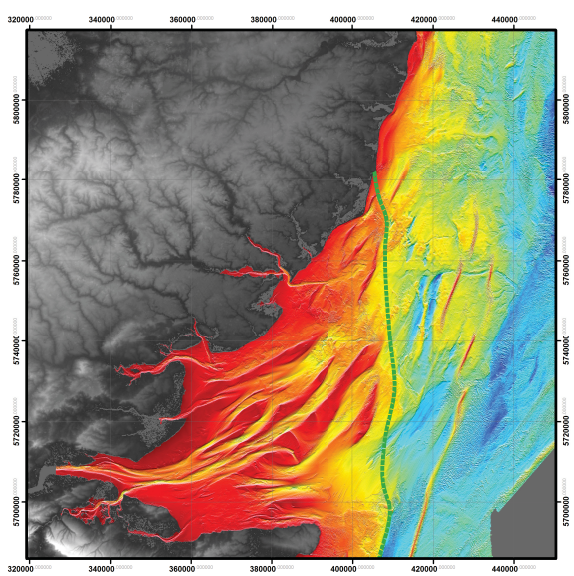

Figure 2 – Bathymetry of the Outer Thames Estuary. Dashed line (green) represents the sub-division of Western and Eastern morphological zones. Depths range from 0 m (red) to -75 m (blue) MSL.

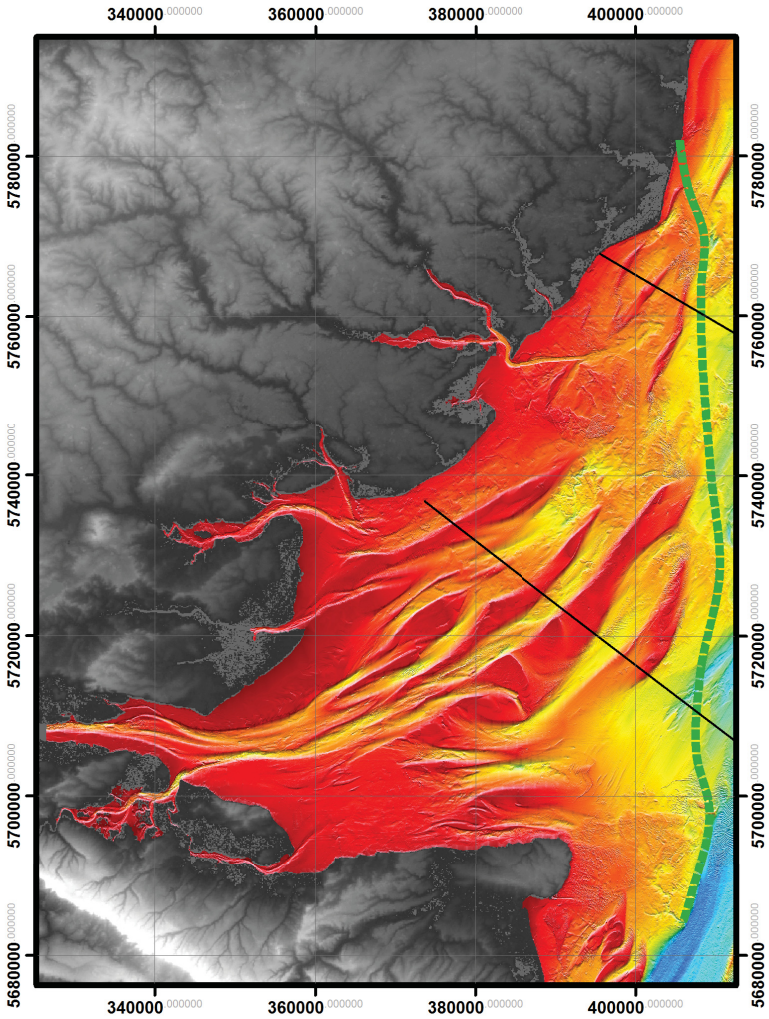

Figure 3 – Bathymetry of the Western Zone. Large sandbanks dominate the region oriented parallel to the coastline. Central black line indicates position of bathymetry profile shown in Fig. 4.

Morphology

The Western Zone is characterised by a series of major sandbanks trending northeast/southwest, parallel to the coast. These banks are typically 1-5 km across and 10-30 km in length, the crests of which are exposed at low water, classified as either wide estuary mouth ridges or estuary mouth banks (Dyer & Huntley, 1999; Burningham & French, 2008). The sandbanks are separated by channels 2-5 km wide which extend as deep as 20 m MSL, the typical depth of the seabed in this region. The eastern margin of the zone has a uniform seabed with depths ranging between 20-25 m MSL, which changes distinctly where it joins the Eastern Zone.

Seabed Character

The large sandbanks have a mostly depositional origin and contain a much thicker succession of sediments than in the Eastern Zone. Twenty-five grab samples from within the Western Zone are composed of seven gravel, sixteen sand, and two mud samples (Fig. 8). The sandbanks themselves are moderately well-sorted fine to medium sands with grain diameter d_{50} of 0.16 mm. There is a distinct change in sediment type along the sandbank margins where the channels are composed of poorly-sorted gravels, sands, and muds up to 1 m thick, with d_{50} of 2.0 mm (REC, 2009).

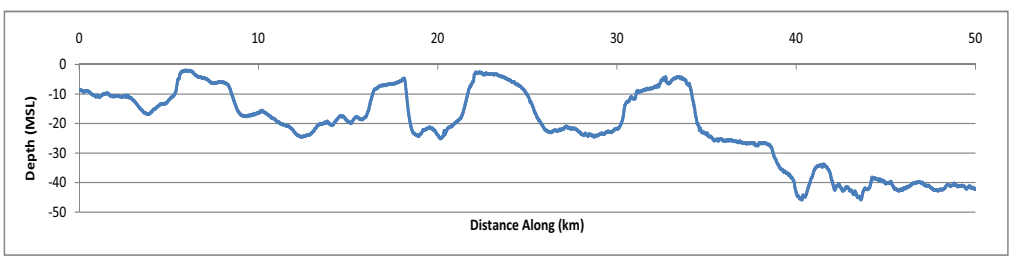

Figure 4 – Bathymetry profile of Western Zone as shown in Fig. 3 (above). Sandbanks can be seen to be nearly exposed at surface, with channels at 20 m depth. At 40 km along-profile the transition in morphology between Western and Eastern Zones is apparent by a change in depth.

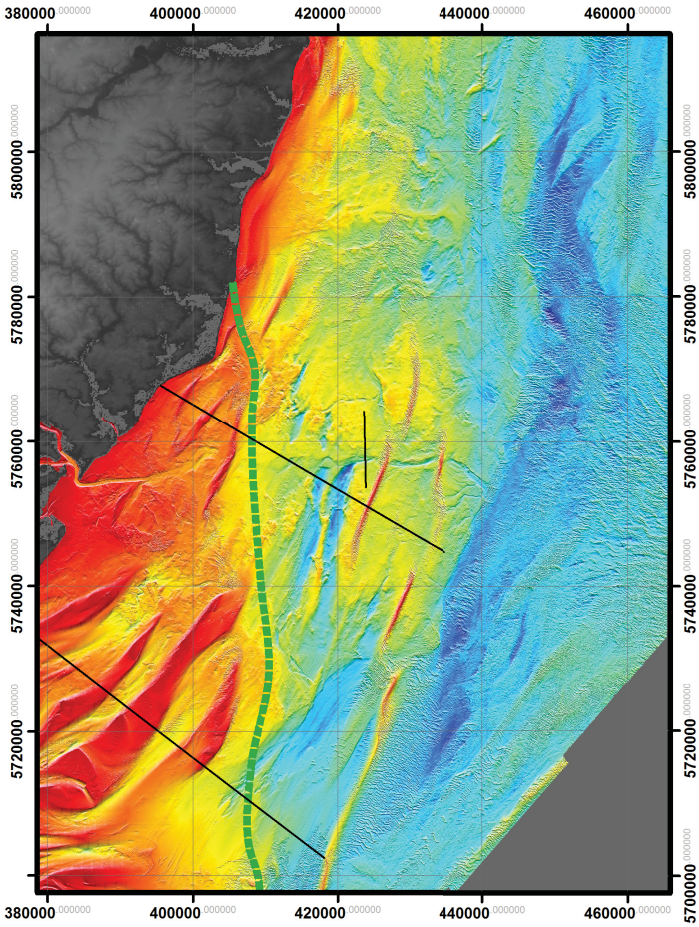

Figure 5 – Bathymetry of the Eastern Zone. Majority of the seabed is a rough, flat platform however isolated sandbanks can be seen trending NNE/SSW parallel to the tidal flow in the region. Long black line indicates position of bathymetry profile shown in Fig. 6 and short black line, Fig. 7.

Morphology

The seabed in the Eastern Zone is a rough but flat platform with several isolated sandbanks and deep troughs. The majority of the platform is between 20-30 m below MSL, but becomes deeper along the eastern margin (Fig. 5). The sandbanks in this area trend NNE-SSW and have elongate dimensions (10 km long, 1-2 km wide), with the crests of these banks typically at 5-10 metres depth. The banks are asymmetrical, oriented parallel to the dominant tidal flow (Kenyon et al., 1981) and are classified as open-shelf ridges (Dyer & Huntley, 1999; Burningham & French, 2008).

Two major troughs approximately 2 km wide and 20 km long interrupt the flat seabed, trending in a north-south direction (Figs. 5 & 6). These troughs are between 20-30 m below the adjacent seabed reaching a maximum depth of c. 60 m (REC, 2009). Smaller troughs of a similar nature can also be seen to the northwest. The other major morphological feature in this zone is an east-west trending channel-like feature with a maximum width of 1 km and depth below adjacent seabed of 10 m (Figs. 5 & 7). This channel is continuous across the middle of the Eastern Zone except where two of the major sandbanks overlie it, hinting at a cross-cutting relationship.

Seabed Character

The Eastern Zone is composed largely of erosional features, with a series of ridges and depressions within a relatively flat seabed. The majority of the zones seabed is composed of sandy gravels and exposed bedrock, often only forming a thin layer overlying the Tertiary bedrock. The gravels and other sediments are believed to be lag deposited during the last sea level transgression, consisting largely of flints sourced from Upper Cretaceous Chalk and Quaternary fluvial deposits (D'Olier, 1975; REC, 2009).

Twenty-eight sample grabs from the Eastern Zone contain nine gravel, twelve sand, and six mud samples (Fig. 8). The majority of the samples are composed of poorly sorted sands and gravels with a d_{50} of 2.00 mm. The remainder of the seabed is covered with sandy sediments composed of fine- to medium-grained sands.

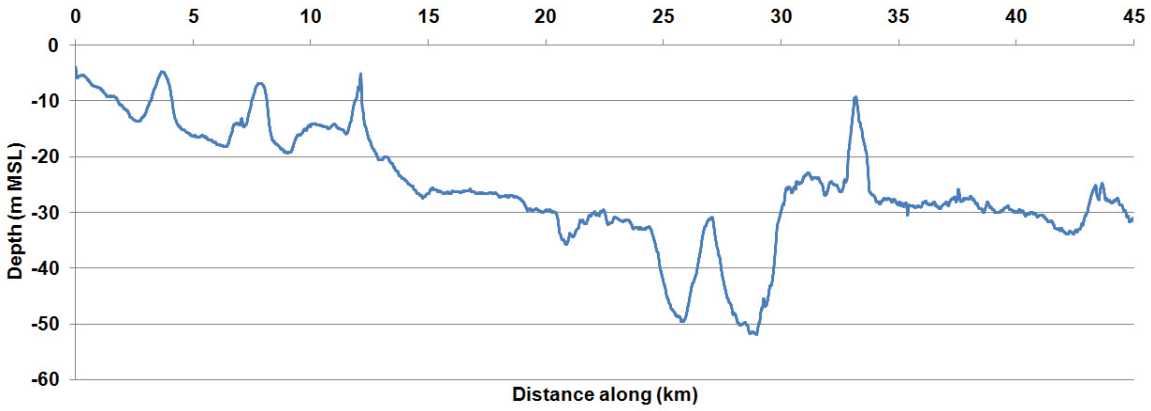

Figure 6 – Bathymetry profile (EW) of Eastern Zone as shown in Fig. 5 (above). Isolated sandbanks cause bathymetric highs, concentrated towards the western end of profile, with two major troughs clearly visible between 25-30 km along-profile.

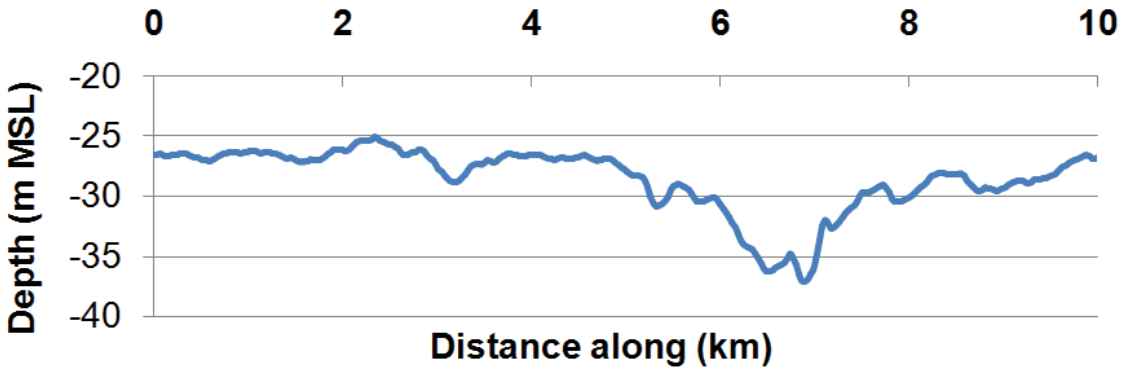

Figure 7 – Bathymetry profile (NS) of Eastern Zone as shown in Fig. 5 (above). Isolated channel-like feature is clearly identifiable at 6-8 km along-profile with maximum depth of 37 m MSL.

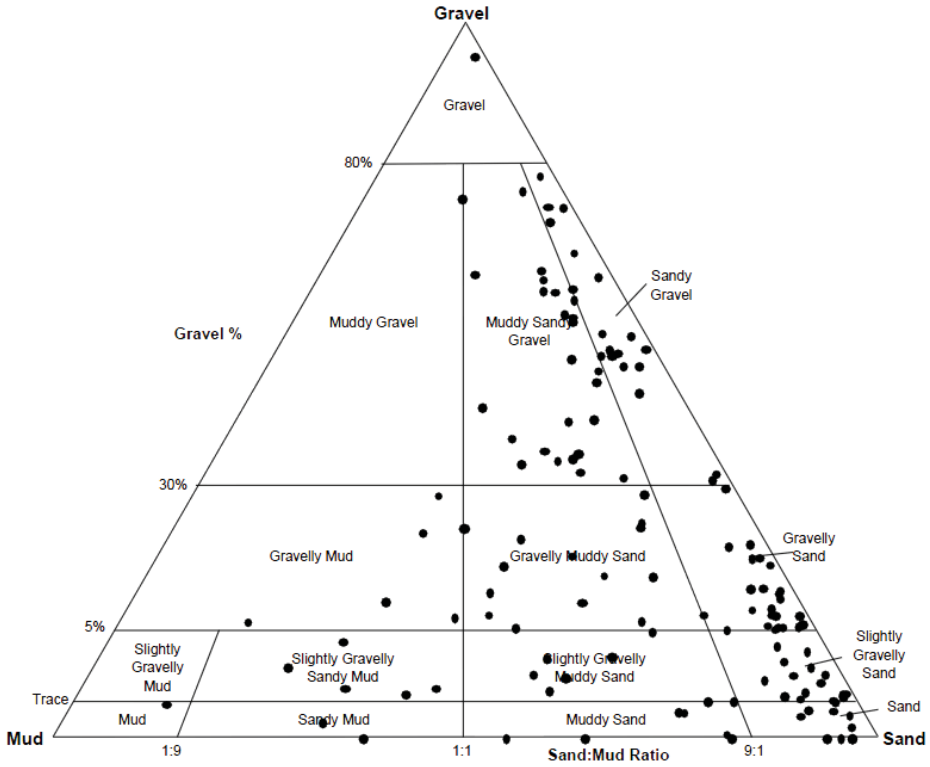

Figure 8 – Sediment classification (Folk, 1954) of the samples recovered during REC 2009 (REC, 2009).

Coastal Evolution

The recent REC survey (REC, 2009) provides a regional overview of the morphological and geological background of the OTE, showing the presence of many active erosional and depositional features. Recent studies of historical bathymetric changes in the Thames estuary (Burningham & French, 2008) present evidence of long-term vertical accretion and erosion which correspond to shifts in sandbank and channel shapes. Additionally large portions of the Eastern Zone are believed to be part of a 'relict' landscape, comprised of a series of Pleistocene age river terraces. These terraces are thought to have formed as a result of lateral movement and downcutting of rivers over multiple glacial/interglacial cycles due to climate changes and tectonic uplift (Bridgland, 2004). Other relict features are believed to be the two major troughs described above, believed to have formed as a result of sub-glacial meltwaters around the Elsterian glaciation (OIS 12). Additionally, the linear channel system has recently been interpreted and dated as a relic river system formed around 720 ka (REC, 2009). The fact that these features are still exposed and relatively sediment-free indi-

cates the possibility that the Eastern Zone is not a signicantly active erosional or depositional region.

Offshore Activity

The OTE is host to several new plans for the development of additional offshore infrastructure, most notably two large wind farms (Fig. 9). The Greater Gabbard wind farm and the larger London Array currently under construction are expected to house up to 140 and 270 turbines respectively which will be situtated among c. 400 km^2 of active sandbanks. Due to the mobile nature of these sandbanks, it is key that risk management and planning officials have access to the best tools with which to predict and quantify the hazards associated with sandbank mobility during the construction and operational phases to the wind farms and associated infrastructure (i.e. pipelines and cabling).

Other offshore activity in the area includes aggregate extraction (Fig. 9). Offshore aggregate dredging is a multi-million pound industry that forms the cornerstone of modern construction, supplying the primary raw materials required for development of new infrastructure. It has become clear that dreding is an operation that has the potential to have significant impact on the marine environment, through destruction of marine habitats and removal of large quantities of sediment. The outputs from this project will be crucial in terms of being able to apply cutting-edge science to develop a larger knowledge base to aid in planning, development, and aggregate licensing for future management of marine aggregate extraction.

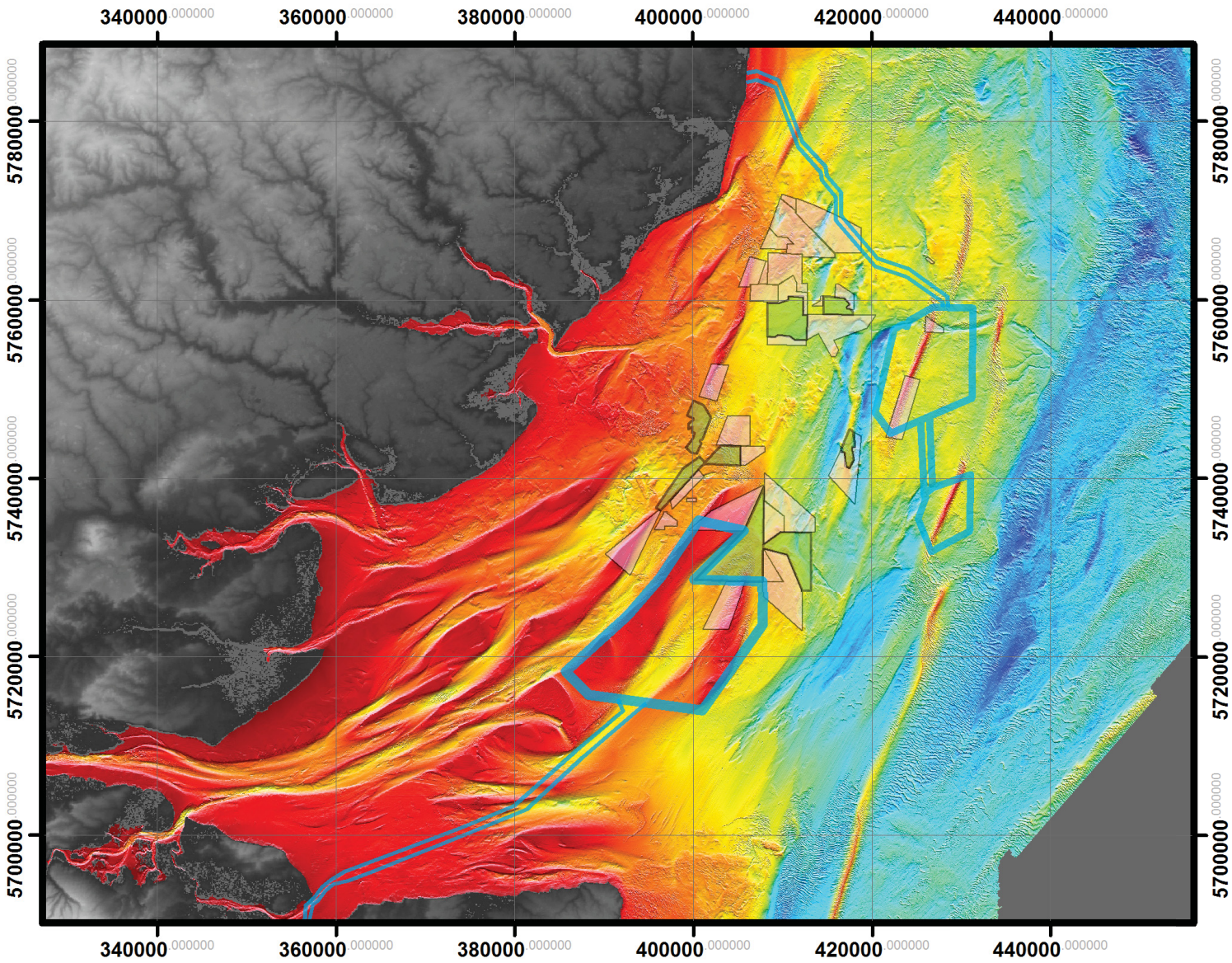

Figure 9 – Summary of major offshore activity in the Outer Thames Estuary. Areas delineated by blue lines indicate regions undergoing development for windfarms, with pink and green shaded areas representing past and currently licensed aggregate extraction zones.

2 Methodology

For this project, the commerical numerical hydrodynamic modelling software *MIKE 21* by DHI (2007) is used in the development of two regional sediment mobility models. The *MIKE 21* software has the ability to model bedload and suspended load sediment transport under a variety of conditions including wave- and tidal-forced currents, in addition to modelling storm events and surges which are known to contribute significantly to sediment flux in the Goodwin Sands and OTE (SNS2, 2002; Dix et al., 2007).

Each sediment mobility model is composed of three individual components. **(1)** The mesh domain **(2)** a hydrodynamic model **(3)** a sediment transport model. For each part of the overall model, a process of iterative calibration is used to test sensitivity of the various parameters and to determine the optimum set of parameters which most accurately replicates the observed hydrodynamics of the region based from available data sources.

2.1 Mesh Design

The first requirement to generate a hydrodynamic model in *MIKE 21* is to produce a 'flexible mesh' over the study area, which is an unstructured grid based on linear triangular elements. This allows for flexibility in the mesh domain in which individual triangular element sizes can be varied as necessary to provide higher resolution over the regions of interest, while maintaining a lower resolution over the remainder of the domain. This is a necessary step in large-scale models, as in this study, because it is computationally unfeasible to model the hydrodynamics at such higher resolutions over such a large area. Initial design of the meshes used in this project required several different inputs including: bathymetry; open water tidal inputs; land/coastline boundaries; and the desired mesh resolution (user-specified). The nature of the final mesh used as an input for the hydrodynamic model is dependent on the required resolution and size of study area, as this will affect the overall runtime of a simulation which can range from hours to several weeks.

The initial aim of this project was to develop a hydrodynamic model over the Goodwin Sands and OTE at a uniform resolution of 25-50 metres, however it became clear after several attempts

that this was impossible given the availibility of computing resources and inherent limitations of *MIKE 21*. A set of stress tests determined the maximum possible resolution over the Goodwin Sands to be 50 metres, however the required simulation time was was c. 50 days and therefore unsuitable. Therefore a mesh domain encompassing the north-western European shelf generated during previous work by Dix et al. (2008) was used to define the boundaries of the model (Fig. 10). Using the refine-by-depth capability in *MIKE 21*, resolution of the mesh was scaled between 20-35 km in the deeper shelf regions to sub-kilometre resolution in the study area. Mesh resolution was also increased through areas of restricted flow to around 5-8 km, i.e. the English Channel, to account for the complexities involved in simulating flow through these regions. As a result, the final meshes used for the project had a resolution over the study region of 100 metres (Goodwin Sands) and 250 metres (OTE) (Fig. 11).

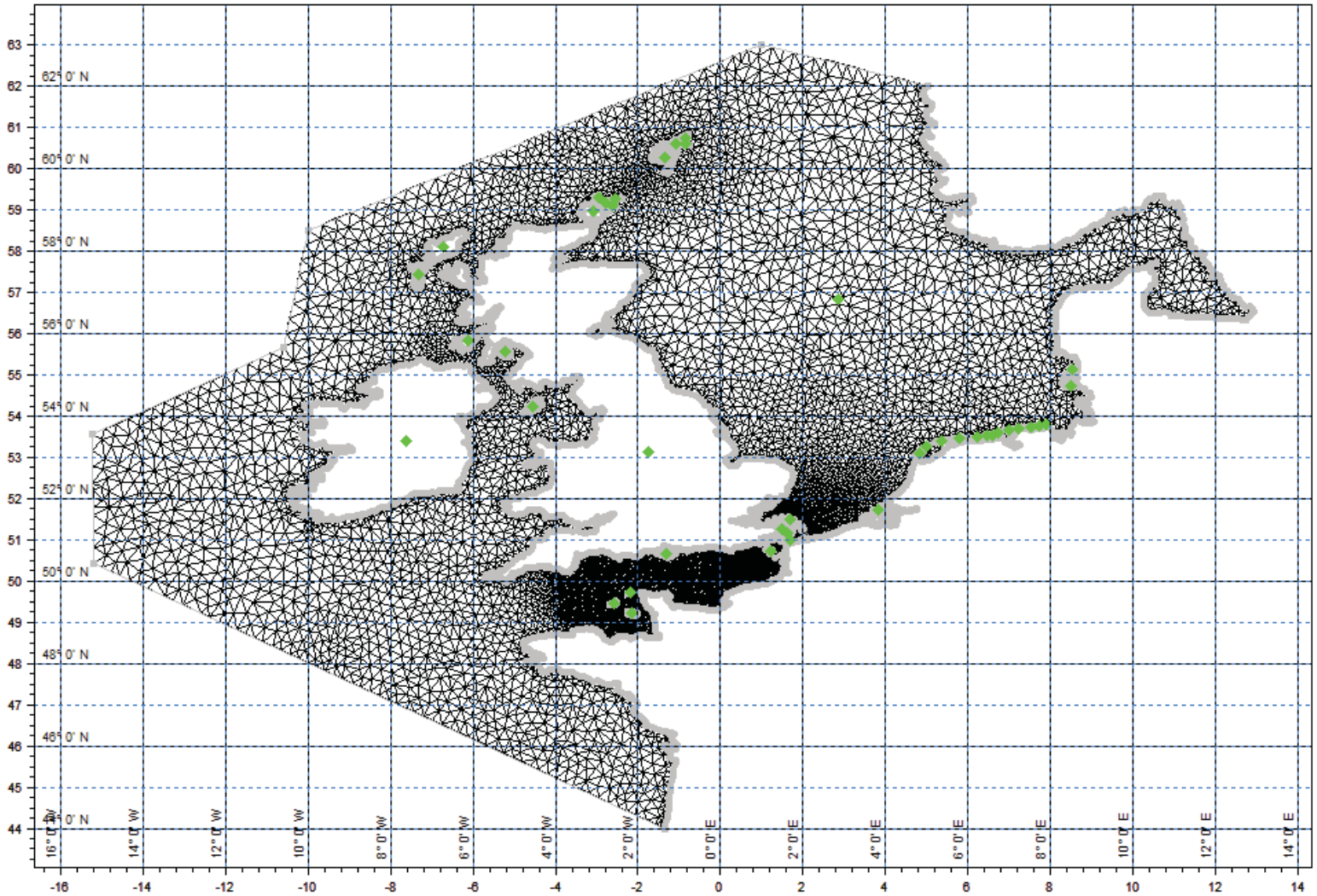

Figure 10 – Extent of mesh domain used in Goodwin Sands and OTE meshes, from Dix et al. (2008). Resolution of triangular elements is 20-35 km in the shelf areas, becoming higher through areas of restricted flow (e.g. English Channel), and towards the southeast of the UK.

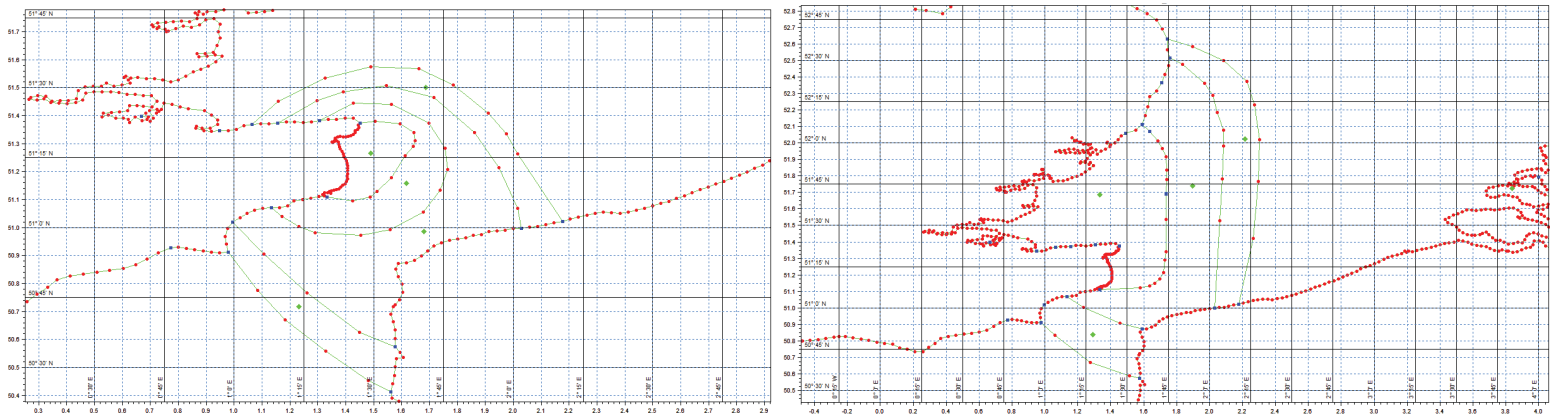

(a) Zoomed view of the mesh domain used for Goodwin Sands. Rings represent resolution zones of 500m, 400m, 200m, 100m (outer to inner).

(b) Zoomed view of the mesh domain used for the Outer Thames Estuary. Rings represent resolution zones of 500m, 400m, 200m, 100m (outer to inner).

Figure 11 – Subset of mesh domain displaying the graded zones of increasing mesh resolution towards study regions.

An additional benefit of using a shelf-scale domain is that it places the model boundaries far from the region of interest, which nullifies any edge effects that may introduce distortion in the flow field of the hydrodynamic model (Fig. 12).

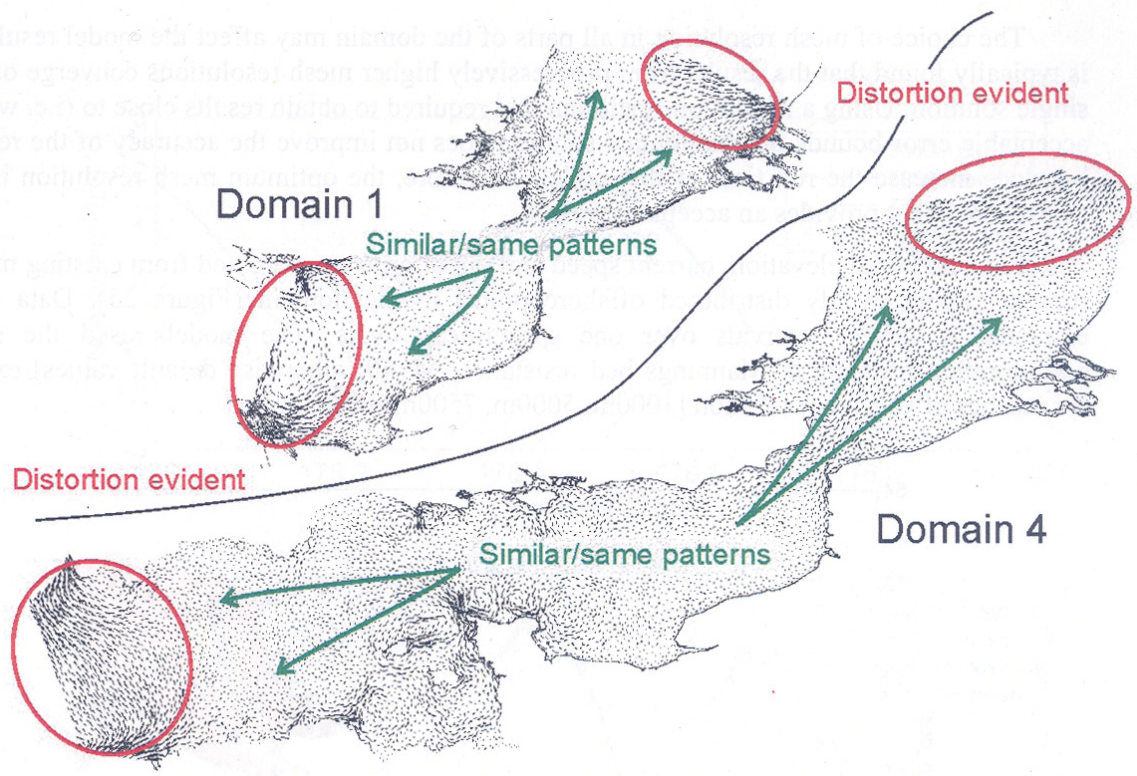

Figure 12 – Example of case where distortion is evident at open boundaries of mesh domain. This effect is nullified by using the large-scale domain described above. *Modified from Dix et al., 2007.*

The final stage of mesh generation involves interpolating gridded bathymetry over the points specified by the triangular mesh. This operation becomes memory-intensive at higher resolutions, which is why the highest resolution achievable for the Goodwin Sands area is 100 metres. The resultant interpolated meshes are then used as inputs for the hydrodynamic module in *MIKE 21*.

2.2 Hydrodynamic Module

The hydrodynamic module in *MIKE 21* provides a set of parameters, for which choices must be made to obtain the best possible estimate of actual hydrodynamic flow. The parameters which can be changed include: the domain that is modelled; the choice of solution technique; bed resistance; and additional forcing mechanisms (i.e. wave and wind). The final choice of parameters is selected through careful iterative calibration against observational data, described in later sections. Based on previous work by Dix et al. (2007), it was found that the following parameters exerted the greatest influence over the end result. Below is a description of these main parameters modified for the hydrodynamic models in this project.

Bathymetry

The bathymetry within the meshed domain is the primary control on propagation of flow. Differences in bathymetry will contribute to an overall different flow field and results associated with it. The overall degree of difference is controlled by the complexity of the region of flow, i.e. over sandbanks or through a constricted region. The bathymetry data used for this project was a high-resolution (20m x 30m) dataset provided by Seazone Solutions Ltd. encompassing the entire OTE and Goodwin Sands, with freely available GEBCO bathymetry providing the remainder of the coverage over the European Shelf at a resolution of c. 2 km.

Flood and Dry

This option allows for the model to simulate portions of the domain which are not continuously submerged as a result of tidal fluctations, i.e. Goodwin Sands. This option was enabled, as it is a well-known fact that large portions of the Goodwins and the banks in the Western Zone of OTE are commonly exposed at low water. This occurs to such an extent, that in previous years cricket matches have been played on the Goodwins themselves. To enable the hydrodynamics to be replicated as realistically as possible, the model should attempt to account for drying out to a similar extent at low tide (Fig. 13).

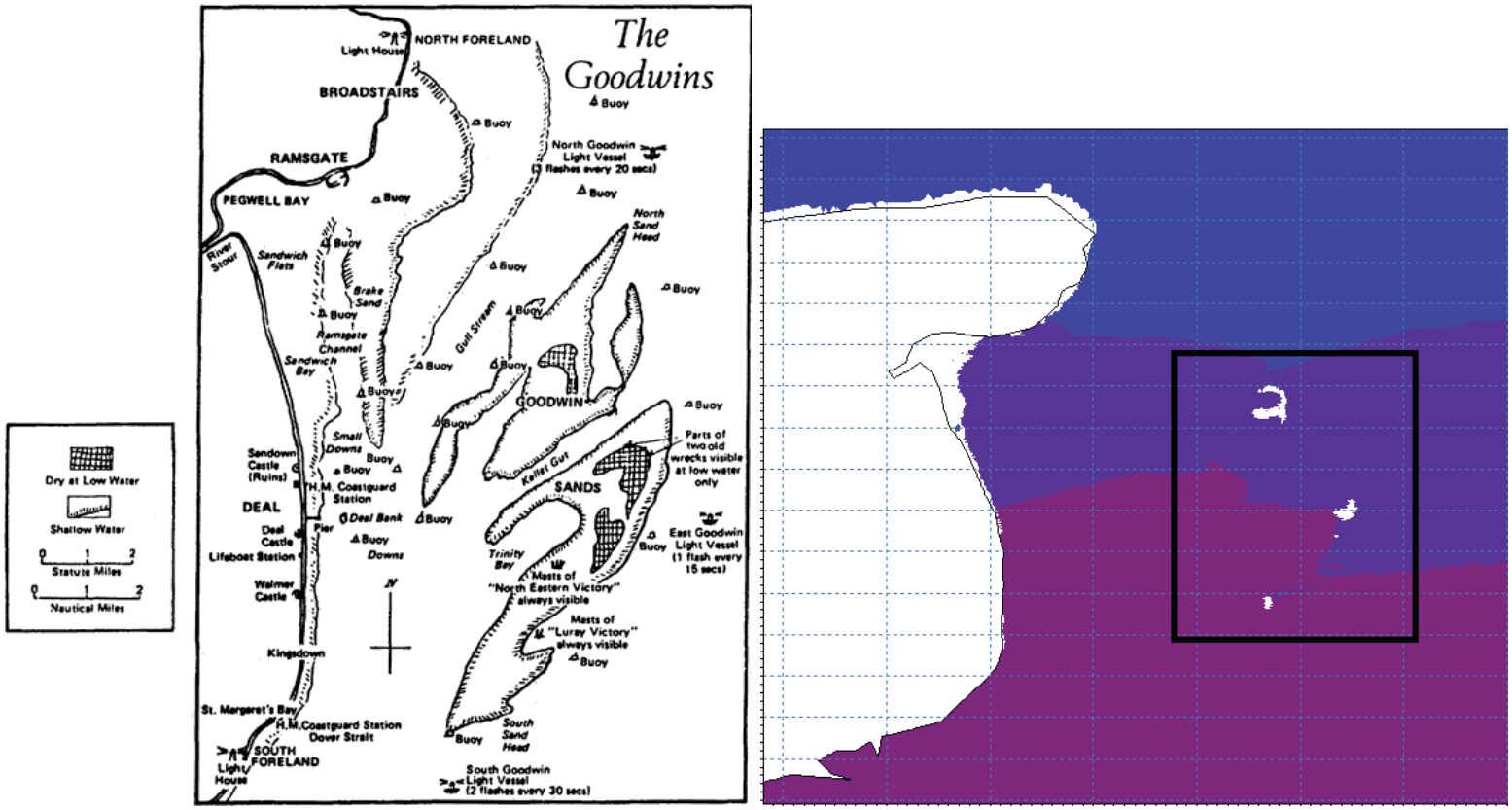

(a) Sketch of exposed regions of Goodwin Sands at low water. *Modified from http://www.whitecliffscountry.org.uk.*

(b) Modelled sea surface elevation, showing regions of Goodwin Sands exposed at low water (black).

Figure 13 – Comparison of observed and modelled exposure of Goodwin Sands during low water for a hydrodynamic model of the Goodwin Sands (see Section 3 for modelling results).

Bed Resistance

Bed resistance is a fundamental parameter which controls flow through the domain by application of friction (bed shear-stress, τ_0) on the water column. Seabed with a smooth surface and bedforms is expected to exert less friction on hydrodynamic flow, and therefore result in higher current speeds. Conversely, a rough seabed with irregular bedforms is expected to exert more friction on flow and therefore lower current speeds. It is key to model current speed as accurately as is possible, due to the relationship between current speed and magnitude of sediment transport. Bed shear-stress is related to the depth-averaged current speed $\bar{U}^2$ by the friction law:

$$\overline{\tau}_0 = \rho_0 C_D \overline{U}^2 \qquad \text{Bed shear-stress} \tag{1}$$

The drag coefficient, C_D, can be calculated using two different formulations in *MIKE 21*. Three styles of bed resistance formulation are available including: Manning number (M), Chezy number (C); or no red resistance (which is physically unrealistic).

$$\mathrm{C}_D = \frac{g}{C^2} \qquad \text{Chezy number (Coefficient, C)} \tag{2}$$

$$\mathrm{C}_D = \frac{g}{\left(Mh^{1/6}\right)^2} \qquad \text{Manning number (Coefficient, M)} \tag{3}$$

As the friction coefficient (M or C) represents the amount of drag placed on the movement of water by the seabed roughness and shape and water depth, by varying this value systematically the overall hydrodynamic flow through a region can be altered. Though it is expected that sediment type, bedforms, and water depth vary throughout a region, *MIKE 21* allows for modelling of either a spatially varying or uniform friction coefficient to be used (Fig. 14). However, the available data for sea bottom typing is not sufficient to generate a mesh that includes spatially varying bed resistance values and as such the uniform formulation is used. Previous work by Dix et al. (2007) within *MIKE 21* shows that variations in friction coefficients M or C exert a significant effect on the propagation of tidal flow and resultant current speed and direction. It was also shown that the

results obtained using either the Manning or Chezy formulations are not significantly different, and as the Manning formulation is the default recommended setting (DHI, 2007), this is the formulation that is used in this project.

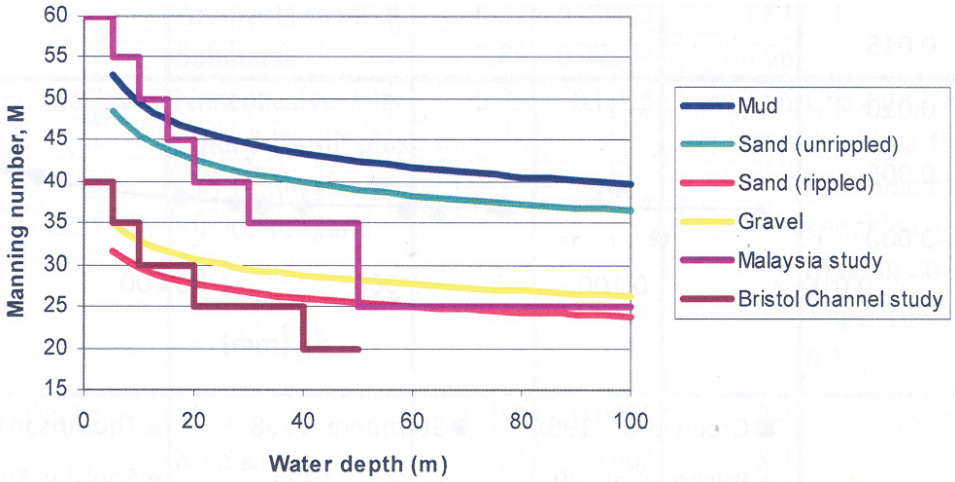

Figure 14 – Variation in the Manning number calculated for varying water depth and seabed type (based on values from Soulsby, 1997). Also, suggested values from calibrated *MIKE 21* studies in order to properly simulate local hydrodynamic processes. *(Figure and caption modified from Dix et al., 2007)*

Given that the Goodwin Sands and OTE are primarily dominated by rippled sands and gravels, at maximum depths of c. 25 metres, it can be seen from Fig. 14 (above) that the range of Manning's number (M) that is applicable for this study ranges between M=27.5 to M=40. All values that are physically unrealistic given what is known about the seabed type and morphology of the study region are discounted from the *MIKE 21* hydrodynamic models.

Extraneous Parameters

Many other options exist which can affect the overall outcome of the hydrodynamic modelling, including the application of wind- and wave-forcing and inclusion of fluvial inputs (such as the River Thames). Given the time frame and established objectives of this project, these additional forcing mechanisms are not explored within as the primary objective is the initial development of high-resolution sediment mobility models. However when examining the results produced from the hydrodynamic models, it must be kept in mind that the exclusion of these additional mechanisms may contribute in part to any deviation between predicted and observed hydrodynamic flow.

2.3 Sediment Transport Module

As with the hydrodynamic module, various parameters can be chosen to model the transport of sands including: model type; sediment transport formulation; bed resistance; and physical sediment properties and distribution. A description of the primary parameters is below:

Model Type

This parameter allows for the selection of a pure current or combined wave and current action transport model, in addition to choices between equilibrium and non-equilibrium flow. As the time frame of this project doesn't allow for the investigation of combined current and wave action, the pure current model was selected. An equilibrium flow response assumes that the sediment in transport is in equilibrium with the flow speed and direction at every time step, while a non-equilibrium response describes a time lag between the flow velocity and observed response in suspended concentration (Dix et al., 2007). As a non-equilibrium response is evidently the more realistic of the two responses, it is the mode used for this study.

Transport Formulation

The mobility of sediments on the seabed is related to the threshold current speed, defined as the velocity at which sediment grains begin to become mobile. The threshold current speed (depth-averaged) required to move a particular grain diameter (d), and subsequent sediment transport can be predicted through the use of various formulations. Though there are multiple formulations, only the van Rijn (1984) formulation for bedload and suspended load transport is used in this project. The previous work by Dix et al. (2007) in the English Channel used the Engelund and Hansen (1972) formulation, which is more simplistic but results in a lower overall propagated error in total sediment transport compared to other formulations. The van Rijn (1984) formulation on the other hand is more complex, but is able to make use of the higher-resolution bathymetric data available while still producing results within 9% of those produced by the Engelund and Hansen (1972) formula (Dix et al., 2007). Given that the variation in the magnitude of sediment transport can differ by up to a factor of 2 depending on which formulation is used, the van Rijn (1984) formulation is

viewed as acceptable for use (Soulsby, 1997).

Sediment Properties

MIKE 21 only supports modelling a single sediment fraction, and therefore only a single representative grain diameter, porosity and relative density can be specified at any one point. The option to include spatially varying grain-diameter is also present, however the porosity and relative density must remain fixed. For the purposes of this study only a uniform distribution of sediment type is used, with multiple grain diameters tested.

2.4 Model Outputs

Outputs from the hydrodynamic model include:

- 2D Surface elevation (1-hr timestep)
- 2D Current speed (depth-averaged) (1-hr timestep)
- 2D Current direction (1-hr timepstep)
- 1D Surface elevation (10-min timestep)
- 1D Current speed (depth-averaged) (10-min timestep)
- 1D Current direction (10-min timestep)

Outputs from the sediment transport model include:

- 2D Bed load (x- and y-components) (1-hr timestep)
- 2D Suspended load (x- and y-components)(1-hr timestep)
- 2D Total load (x- and y-components) (1-hr timepstep)
- 2D Bed level change (cumulative)

The process of calibration based on these results is described in the next Section.

3 Hydrodynamic Calibration

The primary purpose of the hydrodynamic model is to provide the most realistic flow field as possible for input into the sediment transport model. As stated previously, sediment transport only occurs once the threshold current speed is achieved and then in proportion to the excess current speed (above threshold speed) cubed (Soulsby, 1997). Therefore to model sediment transport as accurately as possible, it is necessary to minimize the differences between observed and predicted hydrodynamic flow. In this project, these differences are reduced through a process of iterative calibration through variation of the bed roughness coefficient (Manning number, M).

3.1 Goodwin Sands

Initial calibration was undertaken for the Goodwin Sands mesh, with the final choice of Manning number to be used in generating the hydrodynamic model for the OTE. A range of values for Manning's number were tested, based on suggested values by Cazenave (2010) and those derived from calculations based on water depth and seabed type (Soulsby, 1997).

Table 1 - Summary of parameters used in hydrodynamic models for Goodwin Sands

Mesh Domain	**Manning number (M)**	**Start Date**	**End Date**	**Simulation Length (days)**	**Time Step (minutes)**	**Simulation Time (hours)**
Goodwins	**30**	06/09/1973	01/10/1973	25	10	76.8
Goodwins	**35**	06/09/1973	01/10/1973	25	10	77.9
Goodwins	**40**	06/09/1973	01/10/1973	25	10	77.8
Goodwins	**42.5**	06/09/1973	01/10/1973	25	10	78.0

The time period for which the hydrodynamic models are run is based purely upon the availibility of historical tidal elevation and current meter data within the mesh domain. All data used for calibration was sourced from the British Oceanographic Data Centre (BODC, 2010) website. The locations of available current and tidal stations in relation to the mesh domain is shown in Figure 15.

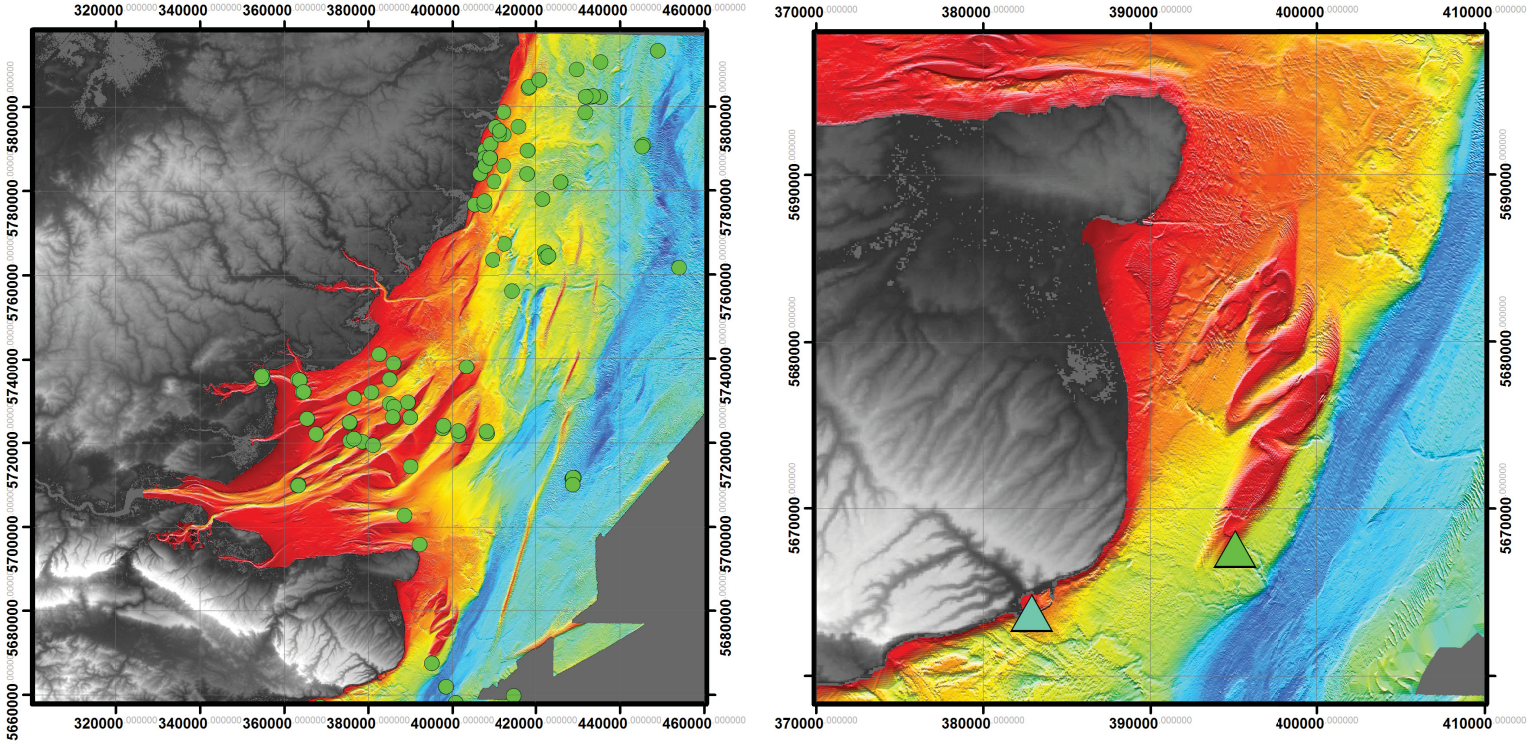

(a) Locations of available current meter data (green) in the OTE.

(b) Subset of Goodwin Sands displaying nearest available current meter (BODC - 14241) and tidal station (Dover).

Figure 15 – Locations of available BODC current (green) and tidal (cyan) meter data within the study area.

Only one BODC current meter is located within the Goodwin Sands, on the southern margin of the South Goodwins (Table 2). Predicted current speed and direction time-series were extracted from each model output at the location(s) listed in Table 2, and predicted tidal elevation time-series were extracted from the nearest tidal station (Dover), show in Figure 15.

Table 2 - Location of BODC current meter(s) used in calibration of Goodwin Sands model

Reference #	**Start Time**	**End Time**	**Sampling Interval (sec)**	**Longitude**	**Latitude**
14241	09/09/1973	25/10/1973	600	1.5000 E	51.1499 N

Calibration of the hydrodynamic model is performed through semi-quantitative analysis of current speed and direction, and tidal elevations. Comparisons between predicted and observed flow speed and direction are made by examining the cross-correlation of the two time-series to first identify any phase lag, and then by examining the absolute difference (residual) between the predicted and observed data. Due to the fact that in some cases the two time-series may have significant phase offset (lag), simply calculating the absolute residual of the data doesn't accurately reflect the actual difference in amplitudes between peak flow velocities and tidal elevations. Therefore when calculating residual differences the predicted time-series is phase-shifted by the phase lag estimated from the cross-correlation, such that peak current velocities and tidal amplitudes coincide between the two datasets (Fig. 16).

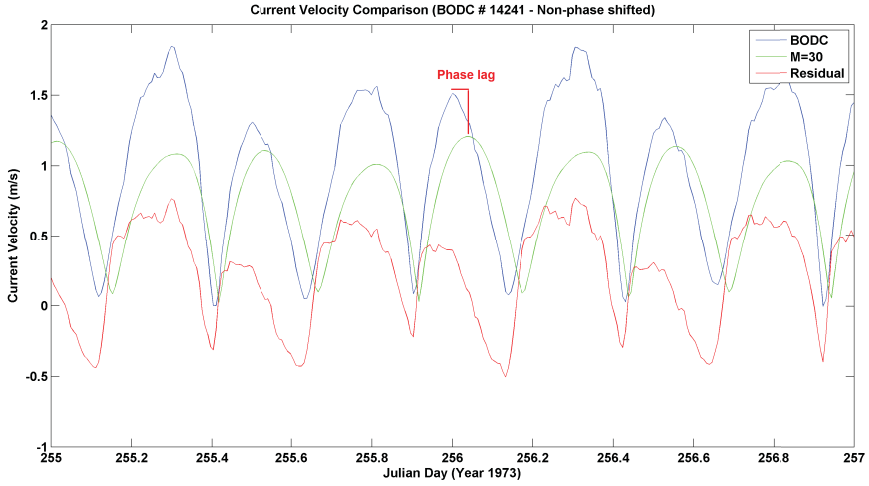

Figure 16 – Comparison of predicted (green) and observed (blue) current velocities with residual amplitude shown in red, for non-phase shifted model M=30. Note the considerable phase lag (c. 30 mins), most evident by the red label.

Several measures of how well each model compares to the observed data are made, some more quantitative than others. The calibration results are summarised in the tables below.

Table 3 - Residual tidal amplitudes for range of Manning numbers at Dover, UK.

Manning number (M)	**Mean Absolute Residual Height (m)**	**Standard Deviation**	**Phase Lag (minutes)**
30	0.4775	0.2818	0 +/- 30 mins
35	0.323	0.1998	0 +/- 30 mins
40	0.201	0.1463	0 +/- 30 mins
42.5	0.17	0.1426	0 +/- 30 mins

Table 4 - Residual flow velocity for range of Manning numbers based on BODC Current Meter 14241

Manning number (M)	**Mean Absolute Residual Velocity (m/s)**	**Standard Deviation**	**Phase Lag (minutes)**
30	0.2435	0.1869	40 +/- 5mins
35	0.1912	0.1549	40 +/- 5mins
40	0.1919	0.1458	30 +/- 5mins
42.5	0.2093	0.1587	30 +/- 5mins

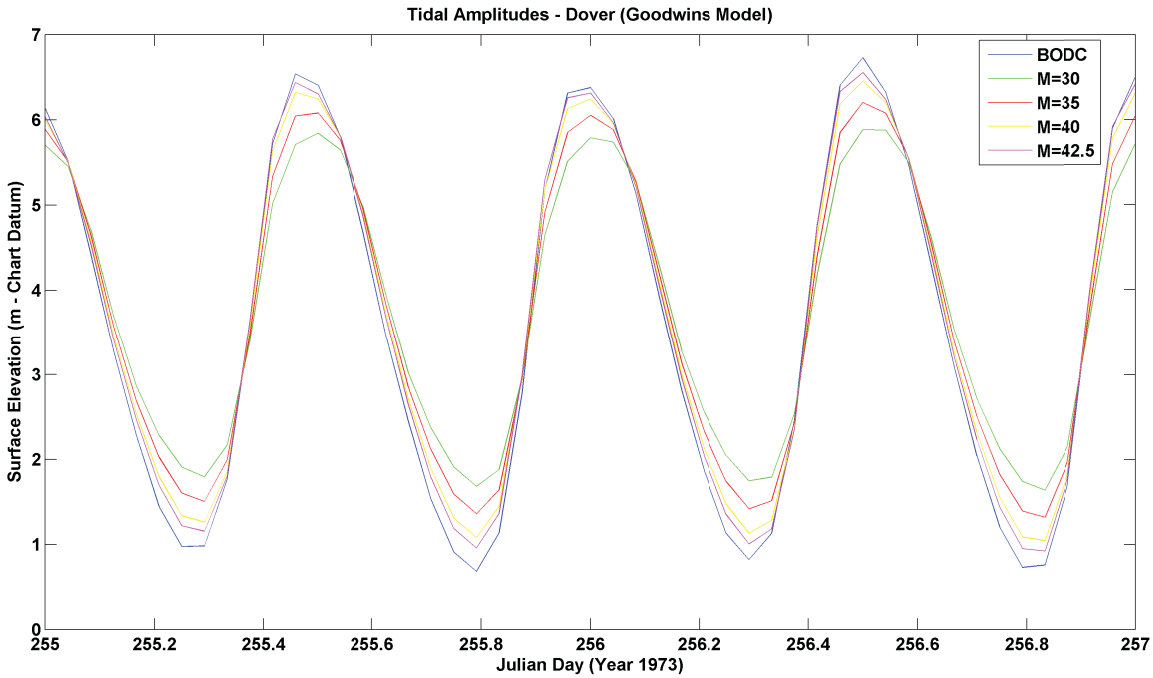

Figure 17 – Comparison of surface elevations from BODC observations (blue) against predicted surface elevations from MIKE 21, over a range of tested Manning numbers at Dover, UK. It can be seen that higher Manning's numbers match the observed amplitudes more closely, with the best match by M=42.5 (purple).

It can be seen by examining model outputs using successively higher Manning's numbers against observations (Fig. 17) that a higher Manning number more closely reproduces the observed tidal amplitudes at Dover, with M=42.5 achieving the smallest mean residual and standard deviation (0.17m +/- 0.14). It appears that predicted tidal amplitudes are highly sensitive to Manning number, with a factor of 2 difference between the amplitudes predicted between M=30 and M=42.5 models. Examination of individual flood and ebb cycles shows that predicted tidal amplitude more closely matches observations during the flood cycle of the tide. This is most apparent for model M=30, where flood cycles have a mean amplitude residual of 0.464 m compared to an ebb cycle mean amplitude residual of 1.026 m, but holds true for higher Manning's numbers albeit with a reduced effect.

Cross-correlation between each model and the observed BODC tidal amplitudes (Fig. 18) shows that the greatest similarity occurs at a phase lag of 0, and therefore the time-series are in phase. However, this is only true to the extent at which the resolution of the time-series occurs. While

predicted tidal amplitudes are calculated at a 10-min interval, BODC tidal observations for the year 1973 at Dover have a resolution of 1 hour. Instead of simply assuming that the two datasets are perfectly in phase, current meter data has also been examined for phase difference (Fig. 21). As BODC Instrument 14241 has a sample rate of 10 minutes, it is most likely that any identified phase lag between predicted and observed current flow is a more accurate representation than phase comparison of tidal amplitudes for this year.

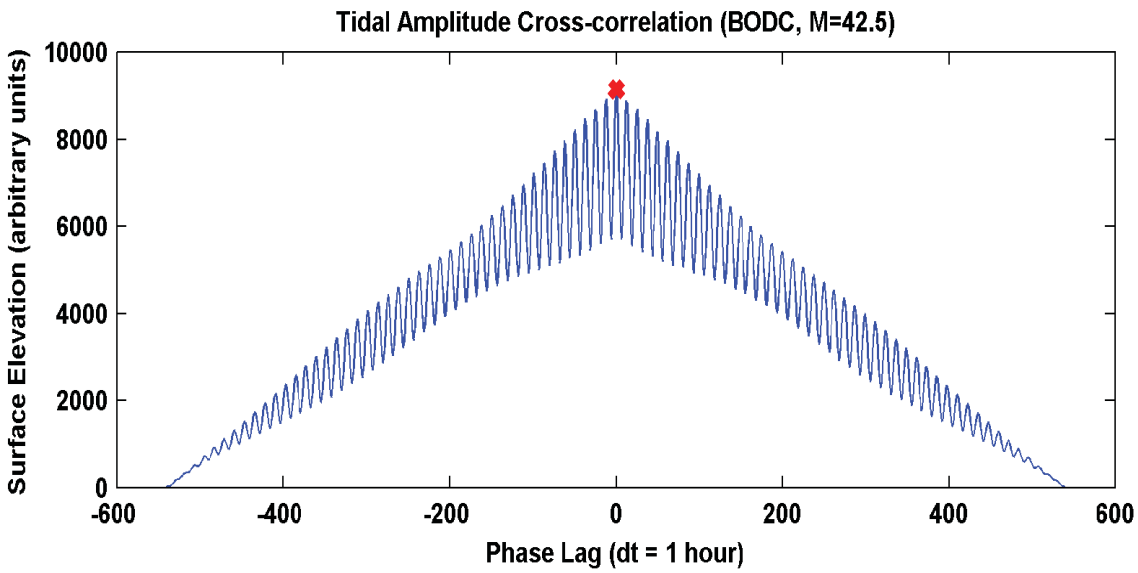

Figure 18 – Tidal amplitude cross-correlation between BODC observations and predicted surface elevations for M=42.5. Maximum correlation between the two time-series occurs at a phase lag of 0, shown by the red circle.

As with tidal amplitude comparisons, the predicted current velocities are highly sensitive to variation in Manning number. Successively higher Manning's numbers result in higher current velocities that more closely match the observed flow (Fig. 19). This agrees with what is expected based on theory as a lower Manning number represents a higher degree of friction being placed upon the water column, acting to reduce the overal current velocity, and vice versa. On the other hand, comparison of current flow directions against observed BODC data (Fig. 20) shows no strong relationship between Manning number and predicted flow direction.

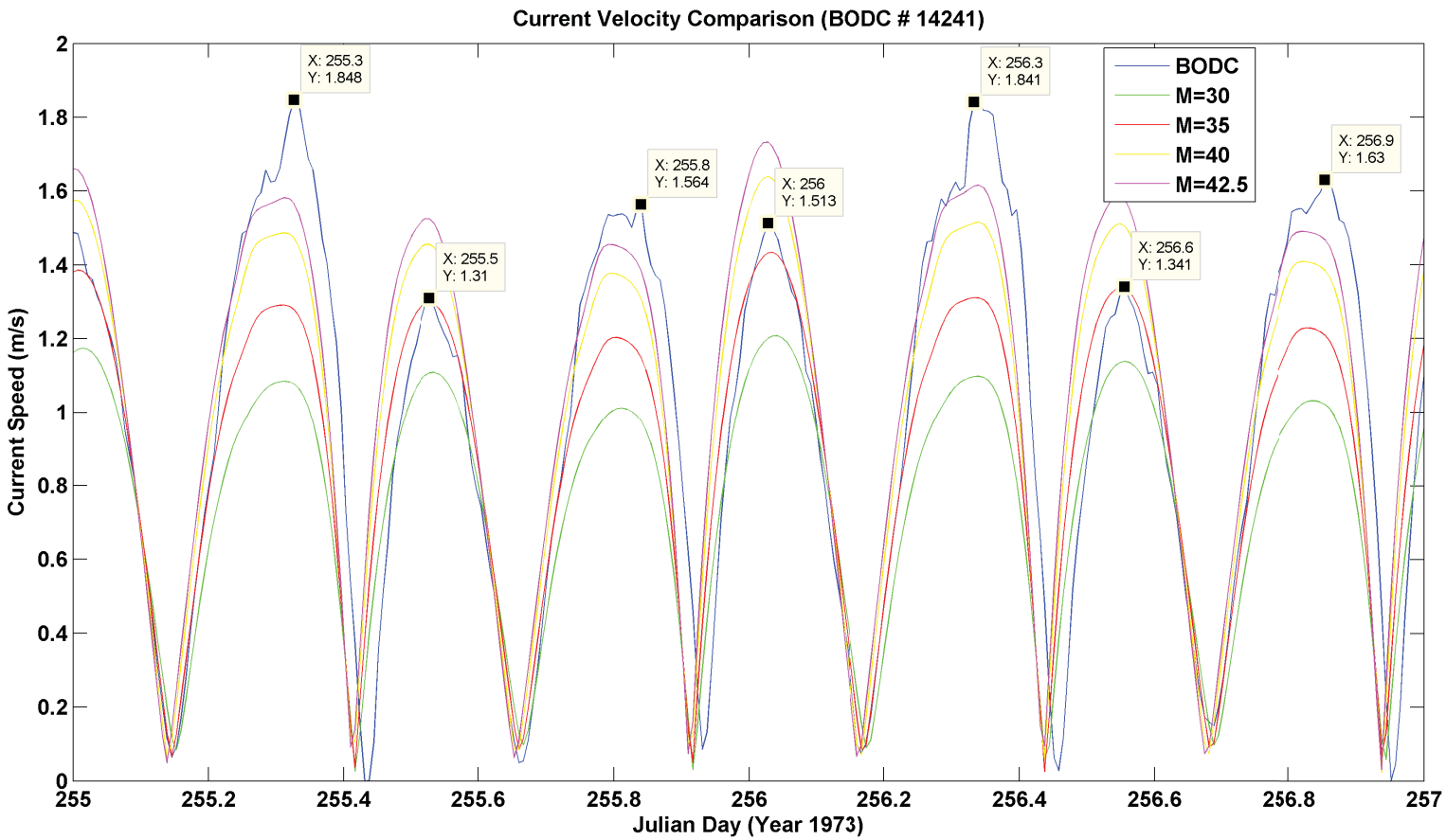

Figure 19 – Current velocity comparison between observed BODC data (blue) and predicted flow velocity for a range of Manning's numbers. Data have been phase-shifted by the phase lag shown in Table 4 so that peak current velocities between observed and predicted flow are coincident. Peak current velocities for each flood and ebb cycle are shown in the callouts.

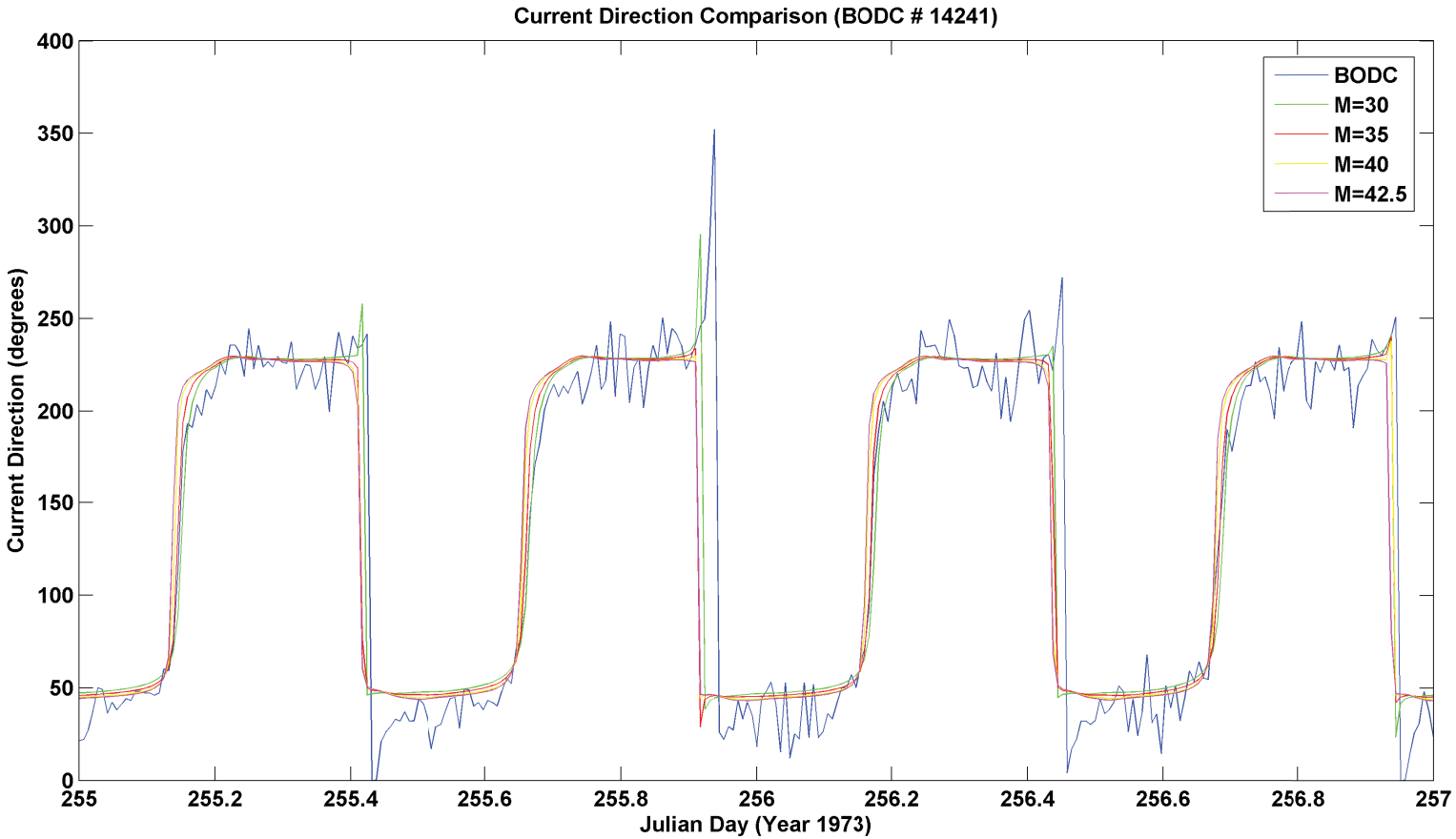

Figure 20 – Current direction comparison between observed BODC data (blue) and predicted flow direction for a range of Manning's numbers. It can be seen that current direction appears much less sensitive to changes in Manning number, with the greatest differences visible during the change in flow direction between each flood and ebb cycle.

Cross-correlation between each model and observed BODC current velocities shows a phase lag of between 30-40 minutes (Fig. 21, Table 4), decreasing with increasing Manning's number, i.e. predicted peak velocities occur 30-40 minutes after peak velocities in observed data. As discussed above, this is a more accurate estimate of the true phase lag than is possible to obtain simply looking at the tidal amplitude time-series.

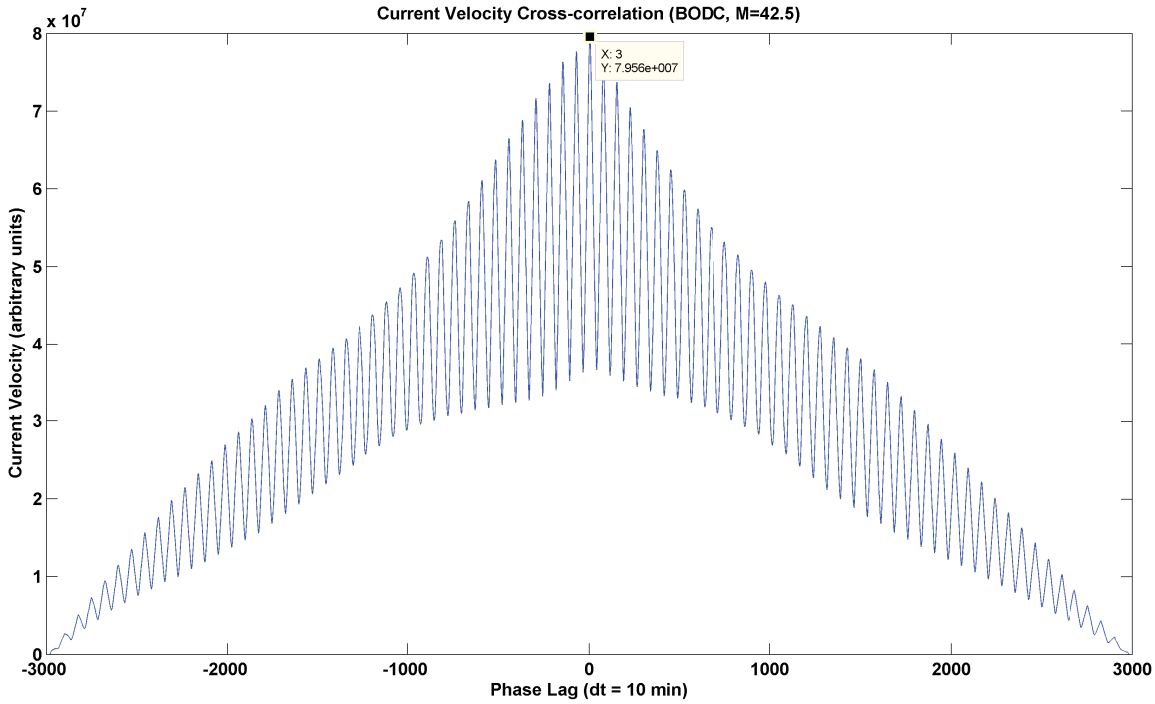

Figure 21 – Current velocity cross-correlation between BODC observations and predicted current velocity for M=42.5. Maximum correlation occurs at a phase lag corresponding to 30 minutes (dt = 3).

Given that predicted current directions show an insensitivity to choice of Manning's number, the Manning number selected for use in the final Goodwins hydrodynamic model and for input into the OTE hydrodynamic model was chosen on the basis of how accurately it models the tidal amplitudes and current velocities. While predicted tidal amplitudes for model M=42.5 most closely match the observations, the same is not true for current velocities. For current velocities, model M=40 provides the most accurate combination of lowest mean residual (0.1919 $ms^{-}1$), standard deviation (0.1458) and phase lag (30 +/- 5mins). As discussed previously the most important parameter to model correctly is current speed, given the highly sensitive relationship between magnitude of sediment transport and excess speed above a threshold value (Soulsby, 1997).

The reason for choosing a lower Manning's number arises from the fact that given what is known about the sediment type in the region, it would be expected that a Manning number closer towards 30 is more suitable for rippled sand (M=32). While theoretically it is highly important to use the most realistic Manning number given the physical conditions of a region, it becomes clear that for the purposes of numerical modelling that only using a higher Manning's number replicates the hydrodynamics accurately. Therefore M=40 was chosen as a trade-off between what is known to be physically realistic and the value that best replicates observed hydrodynamic flow.

3.2 Outer Thames Estuary

The hydrodynamic models calculated for the Outer Thames Estuary use the Manning number obtained from calibration of the Goodwin Sands mesh (M=40). As with the Goodwin Sands model, a suitable time period for which available BODC current meter data exists was selected for the purposes of calibrating the the output of the model. For the OTE only two models were calculated using a fixed Manning's number (M=40), for two seperate time periods. The first model (OTE 1998) runs for 25 days during 1998, the most recent date for which observations are available. However as the OTE covers an extremely large area (5400 km^2) and the most recent data is all located within the Western Zone, a second model (OTE 1972) is also run for 25 days during 1972. This is the most recent date for which current meters with overlapping temporal coverage exist in both the Western and Eastern Zones. The locations of available and selected current meter data and model parameters are shown in Figure 22 and Tables 5 & 6.

Table 5 - Summary of parameters used in hydrodynamic models for OTE

Model	**Manning number (M)**	**Start Date**	**End Date**	**Simulation Length (days)**	**Time Step (minutes)**	**Simulation Time (hours)**
OTE 1998	**40**	29/03/1998	23/04/1998	25	10	39.86
OTE 1972	**40**	10/02/1972	06/03/1972	25	10	39.40

Table 6 - Location of BODC current meter(s) used in calibration of OTE models 1972 & 1998

BODC Reference	**Start Time**	**End Time**	**Sampling Interval (sec)**	**Longitude**	**Latitude**
577721	01/04/1998	16/05/1998	600	1.5983 E	51.7867 N
577677	01/04/1998	16/05/1998	600	1.0317 E	51.525 N
6148	13/02/1972	09/03/1972	600	1.9166 E	52.1833 N
7268	12/02/1972	22/03/1972	600	1.2149 E	51.7133 N
7293	13/02/1972	21/03/1972	600	1.2183 E	51.6266 N
7324	13/02/1972	12/03/1972	600	1.4083 E	51.6749 N
7348	13/02/1972	13/03/1972	600	1.5216 E	51.6533 N

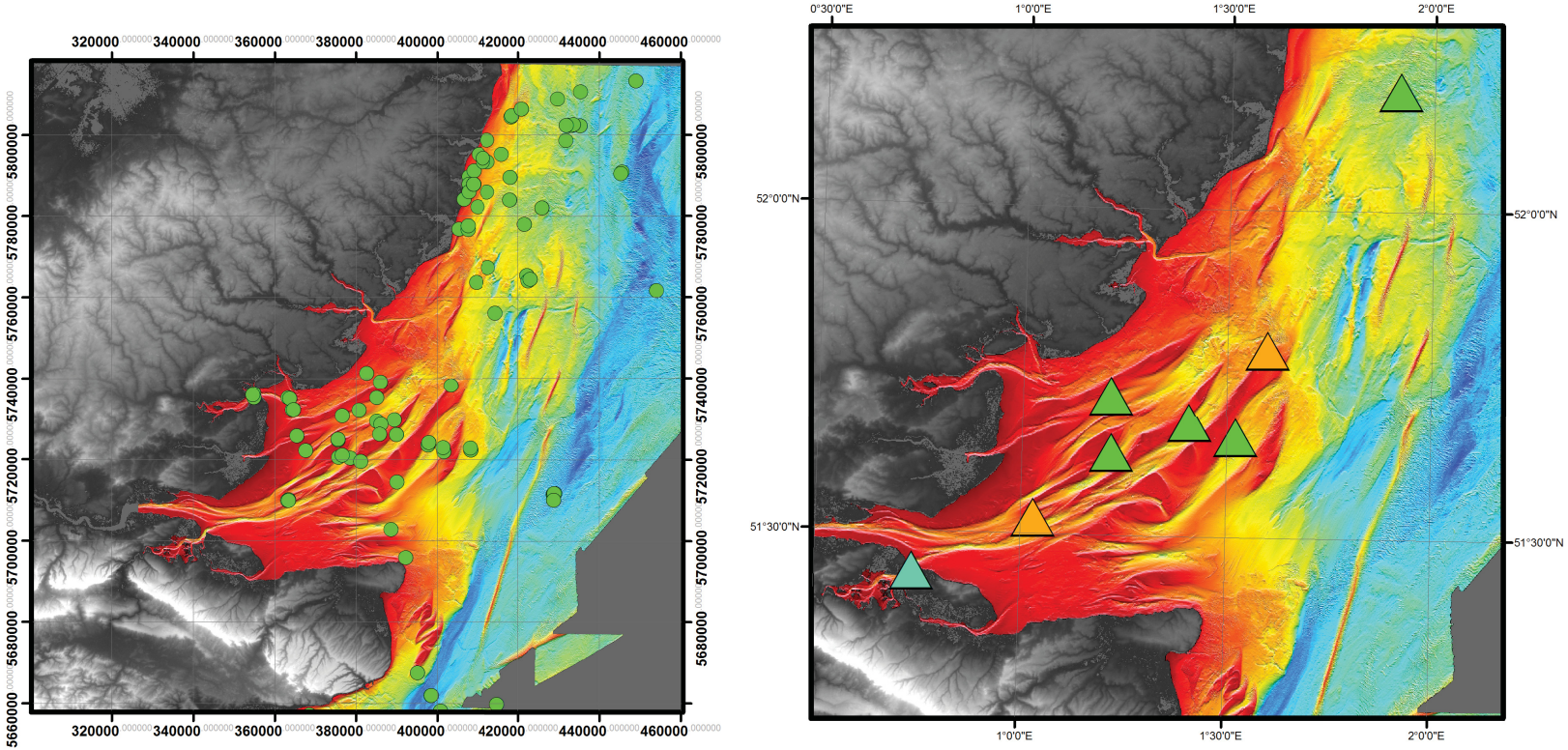

(a) Locations of available current meter data (green) in the OTE.

(b) Subset of OTE displaying nearest available current meters (Table 6) and tidal station (Sheerness).

Figure 22 – Locations of available BODC current (green - 1972, orange - 1998) and tidal (cyan) meter data within the study area.

As before, predicted current velocities and direction time-series were extracted from each 2D model output at the location(s) listed in Table 6, and the predicted tidal elevations extracted at the location of the nearest tidal station (Sheerness) (Fig. 22).

Table 7 - Residual tidal amplitudes for range of Manning numbers at Sheerness, UK.

Model	**Manning number (M)**	**Mean Absolute Residual Height (m)**	**Standard Deviation**	**Phase Lag (minutes)**
OTE 1998	40	0.3673	0.2194	30 +/- 7.5 mins
OTE 1972	40	0.375	0.2422	0 +/- 30 mins

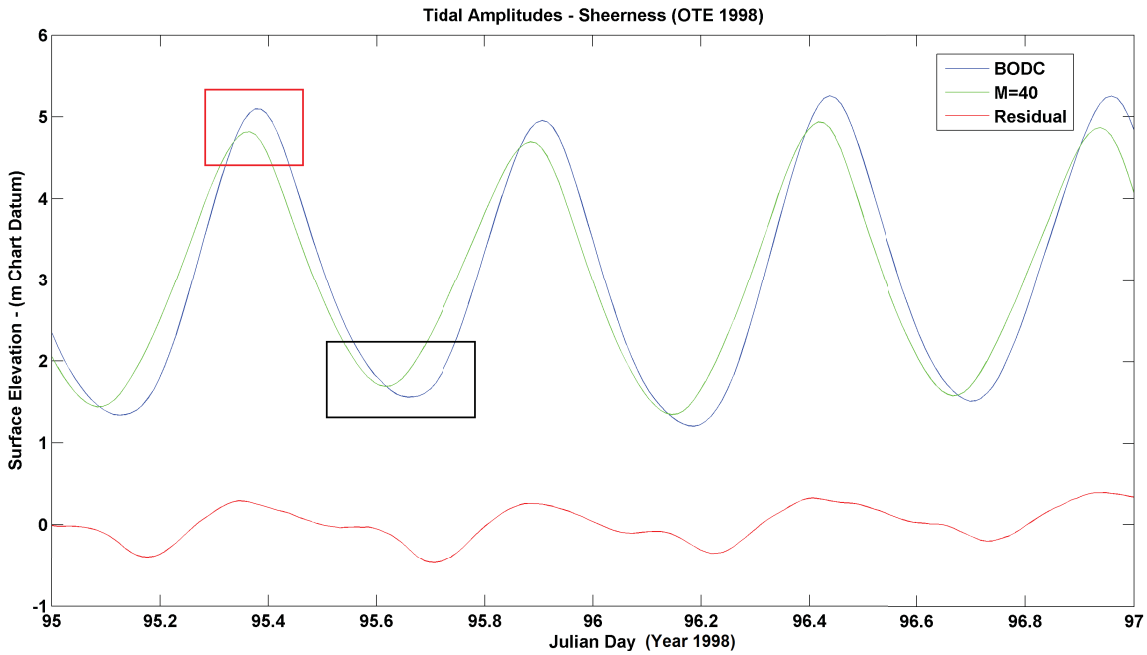

Figure 23 – Comparison of surface elevations from BODC observations (blue, 1998) against predicted values (green) at Sheerness, UK. The residual amplitude difference (red) shows that the ebb cycle of the tide (black) more closely matches the observations (mean ebb cycle residual - 0.109 m) than the flood cycle (red) (mean flood cycle residual - 0.310 m).

The mean residual amplitudes calculated for the 1972 and 1998 OTE models (Table 7) show a signifcantly greater mismatch between the predicted and observed values than found for the Goodwin Sands model, by a factor of c. 2. The results also differ between both the OTE 1972 (Fig. 24) and OTE 1998 (Fig. 23) models. Although both models have a similar mean residual (c. 0.36 m), the OTE 1998 model captures the ebb cycle of the tide (mean residual - 0.109 m) better than the flood

cycle (0.310 m). Conversely, the OTE 1972 model captures the flood cycle best (mean residual - 0.098 m) compared to the ebb cycle (mean residual - 0.653 m).

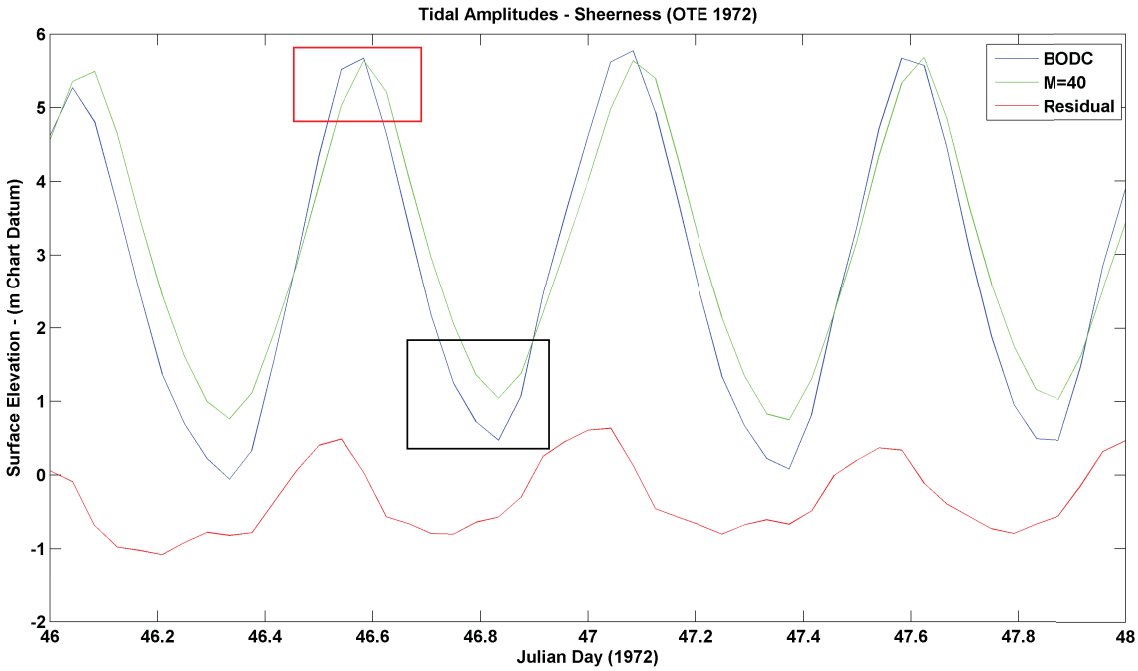

Figure 24 – Comparison of surface elevations from BODC observations (blue, 1972) against predicted values (green) at Sheerness, UK. The residual amplitude difference (red) shows that the flood cycle of the tide (red) more closely matches the observations (mean flood cycle residual - 0.0985 m) than the ebb cycle (black) (mean ebb cycle residual - 0.6528 m).

Phase lag is also evident in the predictions obtained by the OTE 1998 model, due to the more recent data allowing for 15-minute resolution. The estimated lag (40 minutes) from cross-correlation is comparable to the current velocity phase lag calculated for the Goodwin Sands, which indicates that some of the same mechanisms may contribute to the overall differences observed.

Table 8 - Residual current velocities from model OTE 1998

BODC Reference	**Manning number (M)**	**Mean Absolute Residual Velocity (m/s)**	**Standard Deviation**	**Phase Lag (minutes)**
577721	40	0.1234	0.0951	40 +/- 5mins
577677	40	0.0882	0.0629	40 +/- 5mins

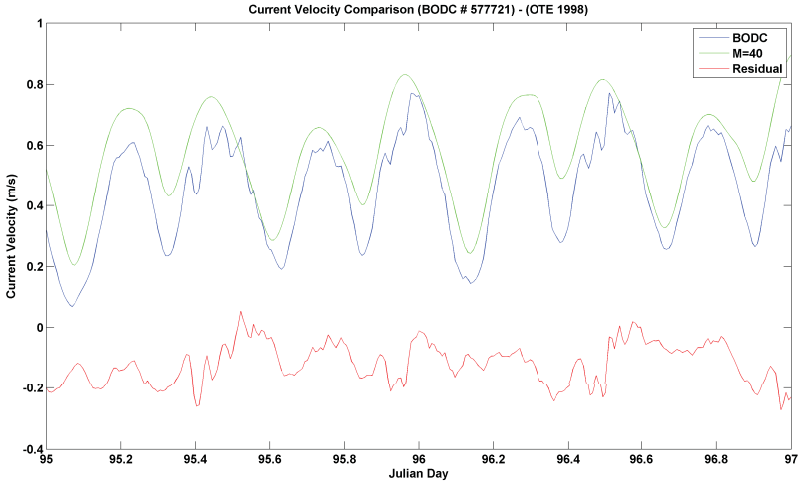

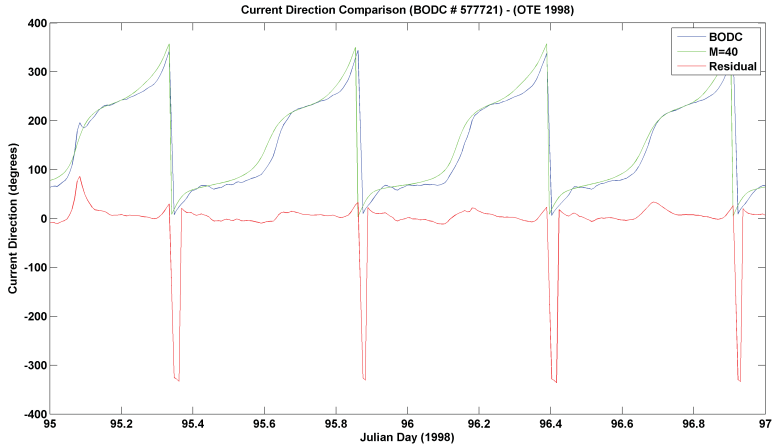

(a) Current velocity comparison between observed BODC data (blue) and predicted flow velocity (green) for model OTE 1998. Residual differences (red) show predicted flow velocities are consistently higher than the observed current velocities. Predicted data have been phase-shifted by the amount described in Table 8.

(b) Current direction comparison between observed BODC data (blue) and predicted flow direction (green) for OTE 1998. The flow direction at this location appears to be NE/SW as expected, however the directional response changes slowly.

Figure 25 – Comparison of predicted (OTE 1998) and observed current velocities and directions (BODC 577721) for M=40.

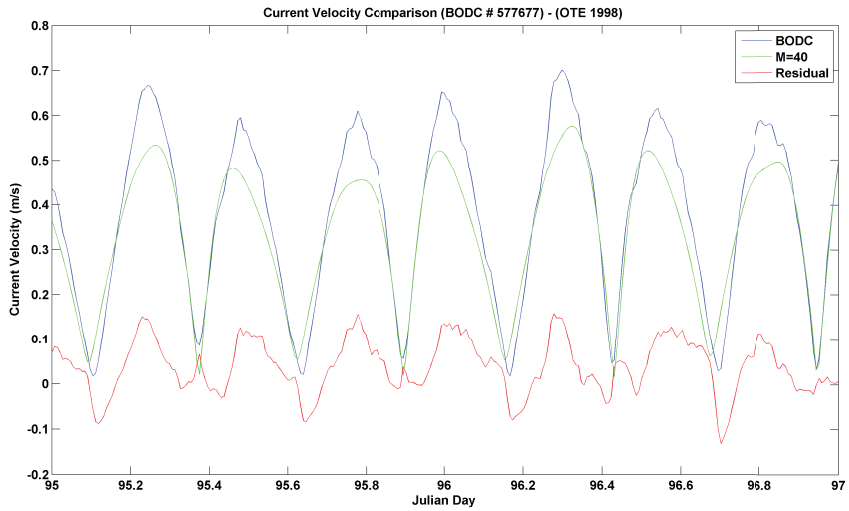

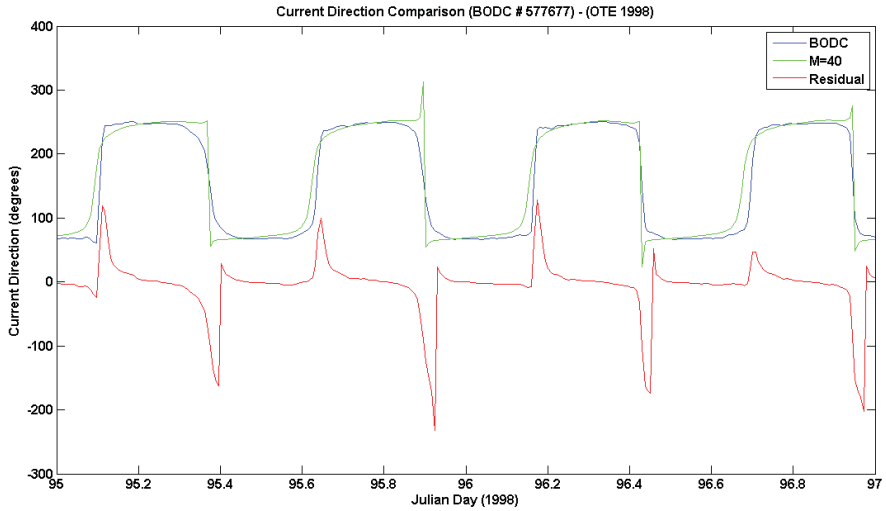

(a) Current velocity comparison between observed BODC data (blue) and predicted flow velocity (green) for model OTE 1998. Residual differences (red) show predicted flow velocities are consistently lower than the observed current velocities. Predicted data have been phase-shifted by the amount described in Table 8.

(b) Current direction comparison between observed BODC data (blue) and predicted flow direction (green) for OTE 1998. The flow at this location is highly directional, flowing NE/SW with only minor deviation (¡ +/- 10 degrees).

Figure 26 – Comparison of predicted (OTE 1998) and observed current velocities and directions (BODC 577677) for M=40.

The same calibration process has been applied to the outputs of the OTE 1972 model, however due to the increased number of calibration sites the results are summarized below in Table 9 and Fig. 27.

Table 9 - Summary of calibration results based on OTE 1972 model.

BODC Reference	**Manning number (M)**	**Mean Absolute Residual Velocity (m/s)**	**Standard Deviation**	**Phase Lag (minutes)**
6148	40	0.0886	0.0649	70 +/- 5mins
7268	40	0.1629	0.1095	60 +/- 5mins
7293	40	0.0953	0.1412	60 +/- 5mins
7324	40	0.1706	0.1383	20 +/- 5mins
7348	40	0.0966	0.0751	40 +/- 5mins

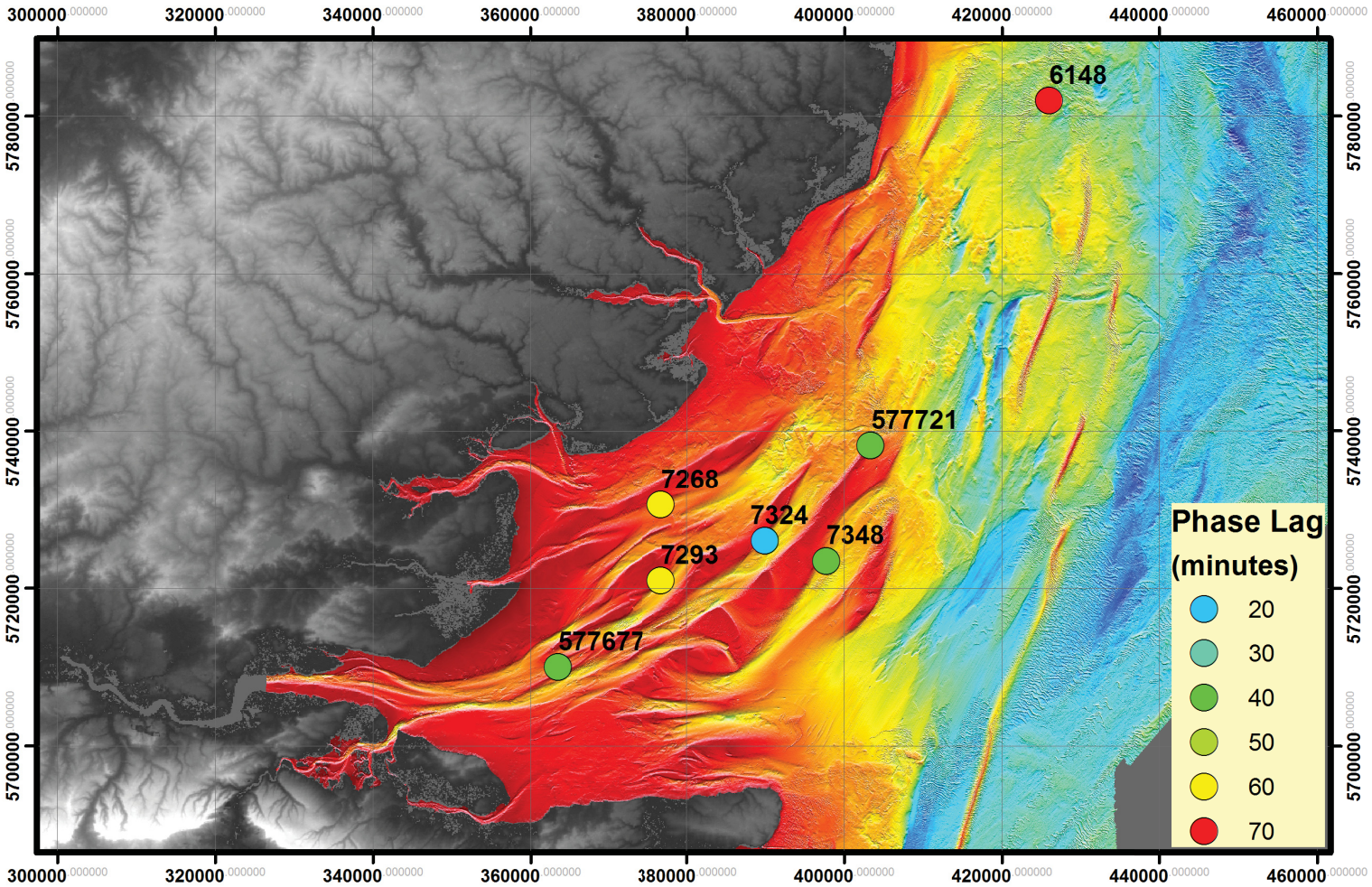

Figure 27 – Spatial variation in phase lag estimated by cross-correlation of current time-series from OTE 1972. There appears to be no correlation between spatial location, mean residual current velocity, and phase lag indicating the possibility of extremely localized hydrodynamic effects.

3.3 Discussion

A simple comparison between the Goodwin Sands hydrodynamic predictions (Tables 3 & 4) and the OTE hydrodynamic predictions for both 1972 & 1998 (Tables 7 & 8) makes it clear that those results obtained for the OTE are not as well-fitting to the observations as those obtained from the Goodwin Sands. Furthermore, while the minimum phase lag for the Goodwin Sands was estimated to be 30 minutes; the phase lags estimated for the OTE are spatially varying between 20-70 minutes (Fig. 27). However, all of the results obtained from the calibrated hydrodynamic models lie within the standard set by the Environment Agency (+/- 10-20% of observed speeds) which indicates that they are of as reliable as other numerical models (Bartlett, 1998). The spatially-varying phase lag and range of residual flow velocities calculated for the OTE in comparison to the Goodwin Sands is that the OTE covers a much larger area (5400 km^2) and a larger range of depths and sediment types while the Goodwin Sands is much smaller in comparison (90 km^2). It could also be proposed that the spatially-variable results indicate a hydrodynamic regime that is quite localized in the OTE due to the complex interactions of fluvial, estuarine, and coastal hydrodynamics.

The most obvious explanation these discrepancies between mesh domains is due to the way in which the physical conditions have been represented and to many degrees simplified for use in the hydrodynamic models. From a theoretical viewpoint, the most obvious source of error introduced through simplication of the physical conditions used in the model is the use of a fixed, non-spatially varying Manning's number. The Manning number represents the friction placed upon the water column by the seabed, which itself is a factor of the shape of the bedforms and the drag they create. However since the highestly resolution of the mesh is only 100 metres in the Goodwin Sands and 250 metres in the OTE, it is impossible to completely and accurately represent these bedforms. This is also one of the reasons for which the use of a higher Manning's number than calculated given physical conditions of the seabed, in order to compensate for the inaccurate representation of the bedforms.

Therefore residual error and phase lag may be reduced by spatially varying the Manning's number at locations where there is signicant deviation from observations. This would serve to increase or decrease flow speed and subsequently the tidal phase and amplitude in a spatially-varying manner to produce more accurate predictions. This method however would also require an entire seperate

stage of calibration, because although varying the Manning number such that it is tailored to the observations, it would only be reliable if the Manning's numbers used correlates with the known sediment grain size distribution and bedforms in a region. This is an aspect of the hydrodynamic model which is not investigated in this project, however will be the subject of future work on this topic.

The secondary cause for observed deviation between predicted and observed hydrodynamics (though an important one), is the exclusion of additional forcing mechanisms (i.e. wind, wave, atmospheric forcing) from the hydrodynamic model. It is obvious that these mechanisms will have an impact to some extent, and possibly a major effect on the tidal amplitudes and current velocities calculated by the model. While not investigated in this project, the previous work by Dix et al. (2008) used a combined tidal and wave flow field to drive their hydrodynamic model which obtained similar residual current velocities for M=40 (i.e. <20 cms^{-1}). Additionally no weather-related events (i.e. storm surges) were taken into account which may contribute to the overall propagated error for the models.

4 Sediment Transport

Using the final calibrated hydrodynamic models for each domain (M=40), a set of sediment transport models were run for a range of sediment properties. As *MIKE 21* can only model sediment transport for a single fraction type, sediment properties representative of the region studied as a whole must be used. For the Goodwin Sands domain the sediment type and properties were kept fixed, using a grain size of 0.38 mm on the basis of previous work (Dix et al., 2008; Cazenave, 2010). In the hydrodynamic models, current velocities are highly sensitive to the Manning coefficient applied to the bed resistance formulation, which has implications for sediment transport. Therefore for robustness, the sensitivity of sediment transport magnitude and direction is also examined by modelling total load transport for a fixed grain size using the van Rijn (1984) formulation.

4.1 Goodwin Sands

Table 10 - Parameters used in sediment transport models for Goodwin Sands

Mesh Domain	**Manning number (M)**	**Formulation**	**Grain Diameter (mm)**	**Simulation Time (hours)**
Goodwins	**30**	van Rijn	0.38	4.2
Goodwins	**32**	van Rijn	0.38	4.4
Goodwins	**34**	van Rijn	0.38	4.1
Goodwins	**36**	van Rijn	0.38	4.6
Goodwins	**38**	van Rijn	0.38	4.3
Goodwins	**40**	van Rijn	0.38	4.3

Two types of output from the sediment transport models are analysed and compared against previous outputs from the MACHU project (Dix et al., 2008) including residual sediment transport (represented with progressive vector diagrams (PVD)) and bed level change. The residual sediment transport vectors represent the net direction and magnitude for which sediment is transported over a single tidal cycle. Analysis of the sediment transport outputs is not straightforward and as previously discussed the resultant magnitudes can vary by a factor of 2 depending on the formulation used. Therefore, any analysis can only be semi-quantitative at best. The units used to describe magnitude of sediment transport are $kgm^{-1}tide^{-1}$, so that they can be compared with previous sediment transport studies such as the SNS (2002) and MACHU outputs.

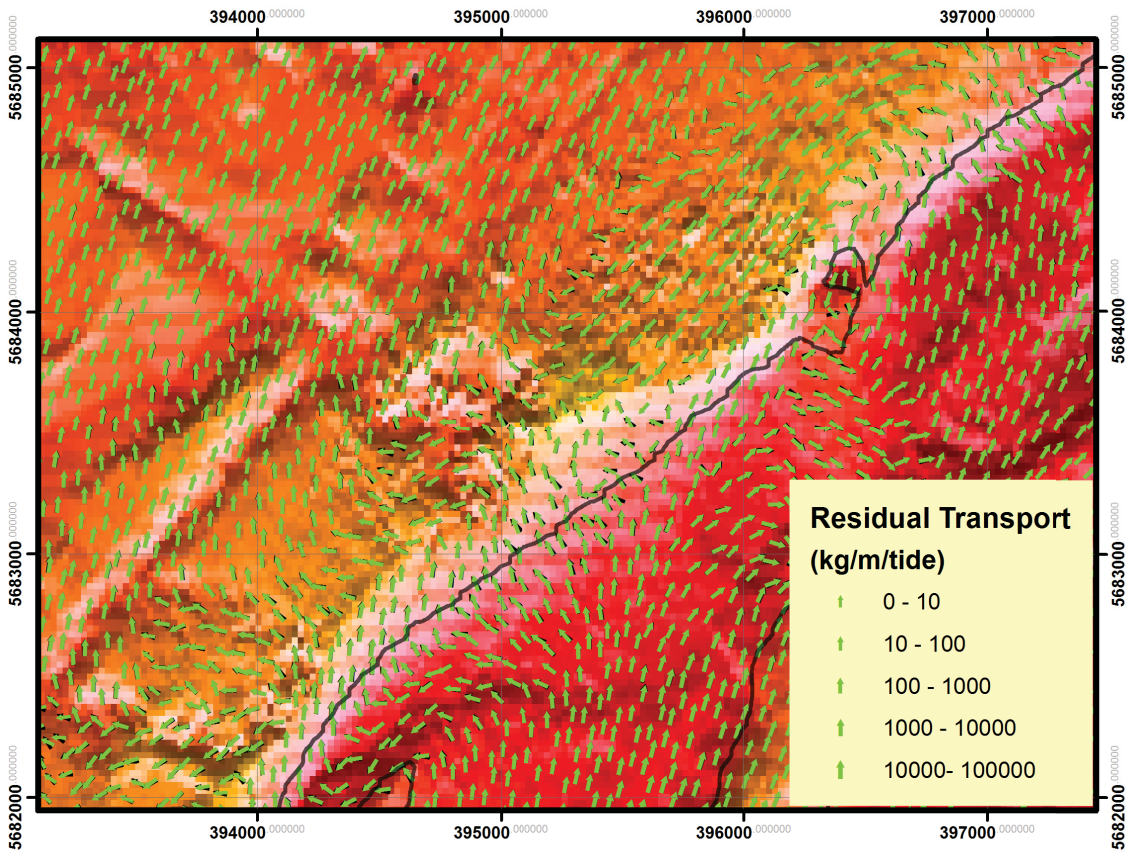

Figure 28 – Representative subset of residual sediment transport vectors for M=30 (green) and M=40 (black) with 10 m depth contour (black) along the northwest margin of North Goodwins. Only minor differences between the magnitude and direction of transport can be identified between the two models, with an overall north and west direction of transport away from the banks.

The sensitivity of residual sediment transport and bed level change to variations in Manning's number is analysed by visually comparing the two end-member values used in model runs (M=30 & M=40). It can be seen that there is little variation in either magnitude or direction of residual transport between each end-member (Fig. 28 & 29). Examination of the entire Goodwin Sands region shows that any differences between the magnitude or direction of transport are concentrated in regions of complex flow such as convergence or divergence zones along the margins of the banks.

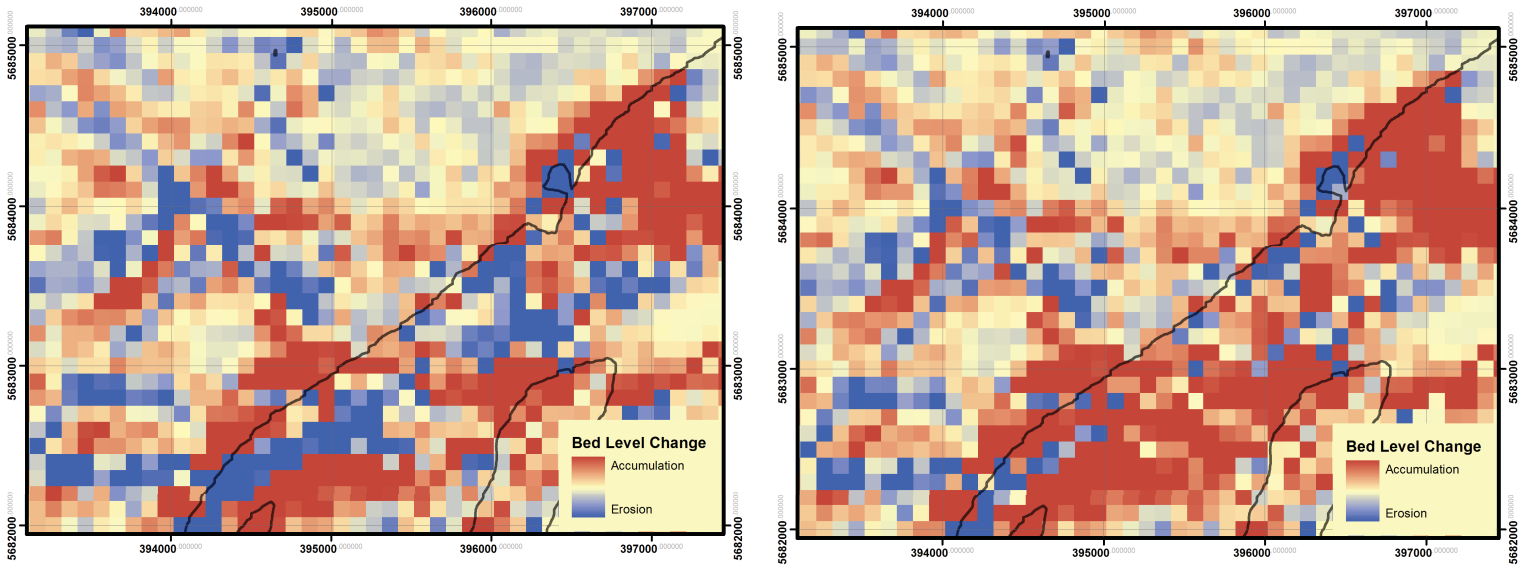

(a) Predicted relative bed level change estimated for M=30. There appears to be enhanced accumulation and erosion along the tops and margins of the banks, with reduced accumulation and erosion along the adjacent seabed.

(b) Predicted relative bed level change estimated for M=40. There appears to be a stronger accumulation component alogn the tops and margins of the banks than for the M=30 model.

Figure 29 – Comparison of bed level change estimated for M=30 and M=40 on the north-west margin of North Goodwins, with 10 m contour (black). While some differences exist, the general trend of areas of erosion and accumulation appear to be similar between both models.

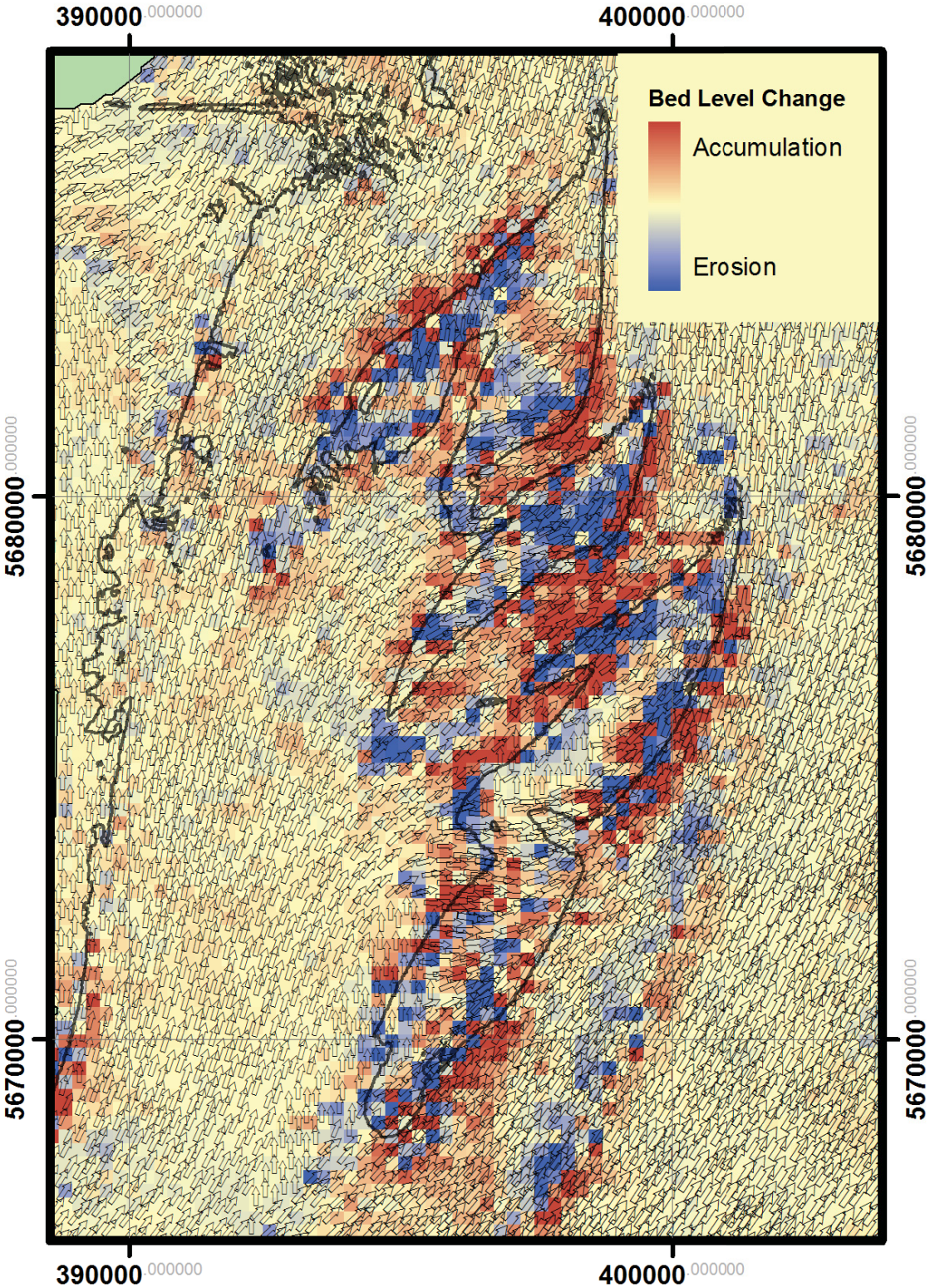

Figure 30 – Bed level change for the Goodwin Sands as calculated by Dix et al. (2008) gridded at 250 m resolution combined with residual transport vectors.

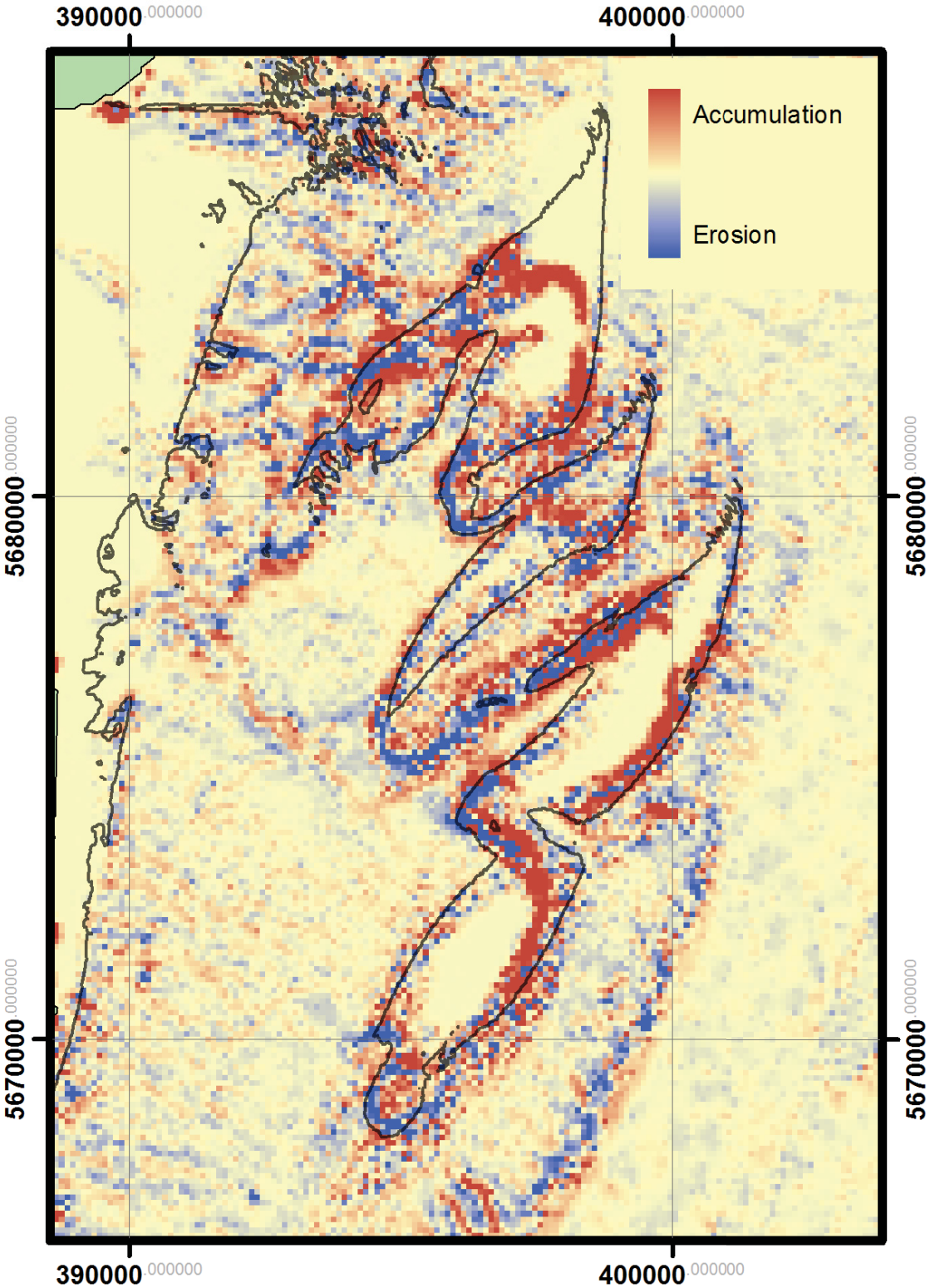

Figure 31 – Bed level change for the Goodwin Sands as calculted from the sediment transport model M=30, gridded at 100 m resolution. Residual transport vector comparison with MACHU outputs are shown in Fig. 32.

An additional source of calibration can be seen by comparison of swath bathymetry obtained over two wreck sites (Fig. 33) where flow-normal bedforms indicating net transport in a NNE direction agree with the predicted directions. As such, the 3 wreck sites near this area can be describe as being in areas of undergoing relatively low rates of bed level change with a small degree of erosion, rather than accumulation as predicted by the MACHU outputs. This discrepancy may only be due to the resolution difference between the datasets, as the agreement of sediment transport vectors indicates a good fit between the two models.

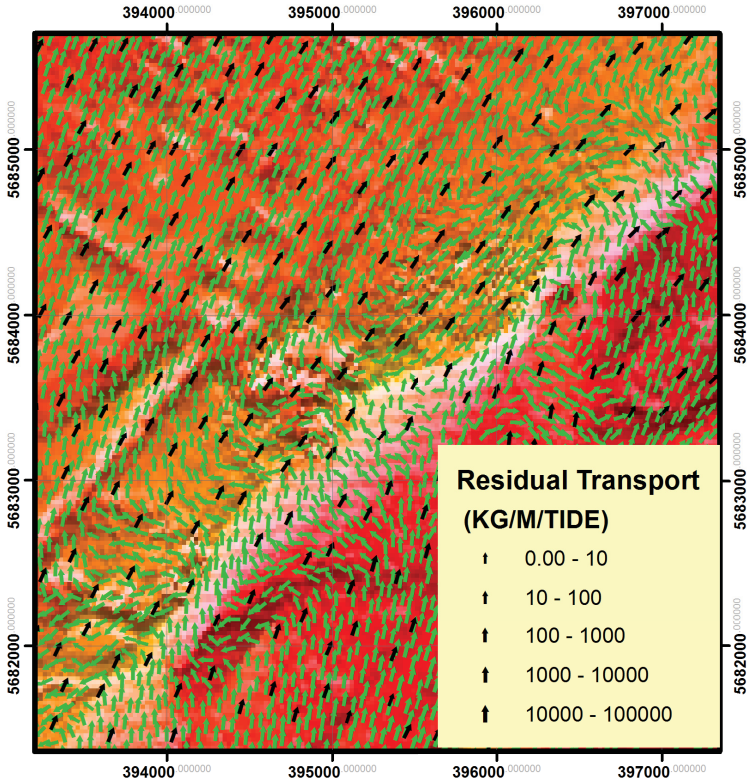

Figure 32 – Representative comparison of residual sediment transport direction and magnitude from model M=30 (green) and MACHU outputs (black) along the northwest margin of North Goodwins. There is general agreement in the large-scale directional transport towards the NNE.

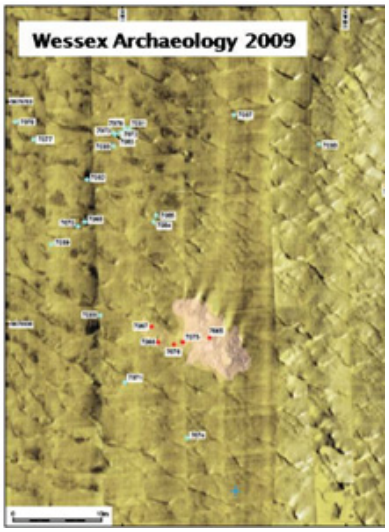

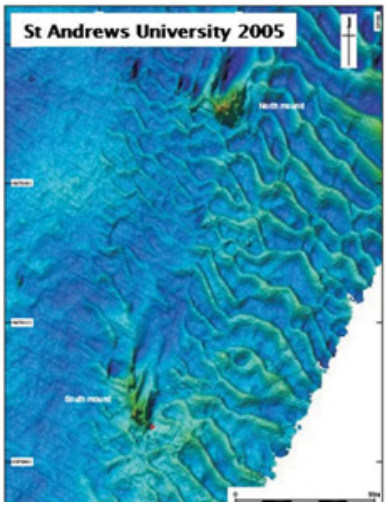

(a) Swath bathymetry data of the Northumberland.

(b) Swath bathymetry data of the Restoration.

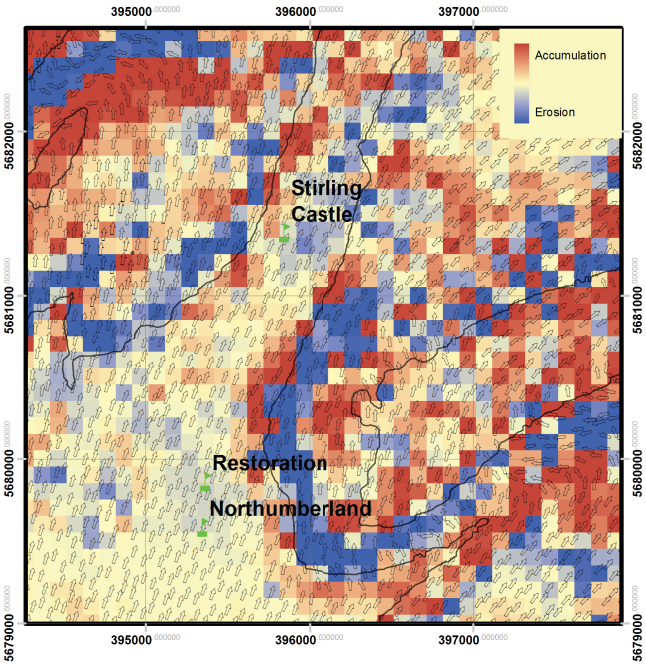

(c) Predicted bed level change overlain with residual sediment transport vectors near multiple wreck sites.

Figure 33 – Comparison between swath bathymetry and sediment transport model results shows agreement between bedforms oriented normal to the flow direction (NNE).

4.1.1 Discussion

Comparison between the outputs of previous sediment transport models in the Goodwin Sands (Dix et al., 2008) and the higher resolution predictions obtained in this project shows a remarkable improvement in the detail of transport direction and regions of erosion and accumulation. The overall northwards transport predicted by Dix et al. (2008) for the Goodwin Sands (Fig. 30) is seen to be replicated on a higher resolution from the outputs of this project (Fig. 32), with small-scale deviations likely due to the increased resolution of the hydrodynamic model. The patterns of accumulation and erosion (Fig. 31) seem to indicate an overall northwards and westwards movement of the northwest margin of the North Goodwins. Along the south and southeast margins of the South Goodwins, strong patterns of accumulation and erosion seem to indicate overall south and east movement. These results coupled with residual sediment transport directions reproduce the findings of Dix et al. (2008) and show the possiblity for anti-clockwise rotation of the Goodwin Sands as predicted by Cloet (1954).

Calibration of these results against high-resolution swath bathymetry shows general agreement between both the MACHU outputs and the observed bedforms. It is important to remember that calibration of the sediment transport is only possible in the few places where observational data exists and the results may have spatially variable accuracy, which naturally has implications for any regional-scale conclusions drawn from the model outputs. Therefore for any application requiring the advanced calibration or prediction of sediment transport volumes it is necessary to generate a model that is calibrated towards site-specific measurements especially when considering the variation in magnitude dependant upon the type of formulation used.

4.2 Outer Thames Estuary

The Outer Thames Estuary represents a much larger region with variable morphology and sediment coverage. As such two end-member sediment transport models are run using the mean grain size of the major sandbanks (0.16 mm) and the Eastern Zone (2.00 mm). This allows for an initial analysis of sandbank mobility similar to that by Burningham & French (2008), as well as determining if the hydrodynamics at present support an active depositional or erosional environment in the Eastern Zone, and whether they contribute towards preservation of the possible relict landscape (Bridgland, 2004).

Table 11 - Parameters used in sediment transport models for OTE

Mesh Domain	**Manning number (M)**	**Formulation**	**Grain Diameter (mm)**	**Simulation Time (hours)**
OTE 1998	**30**	van Rijn	0.16	4.2
OTE 1998	**32**	van Rijn	0.16	4.4
OTE 1998	**34**	van Rijn	0.16	4.2
OTE 1998	**36**	van Rijn	0.16	4.6
OTE 1998	**38**	van Rijn	0.16	4.1
OTE 1998	**40**	van Rijn	0.16	4.4
OTE 1998	**30**	van Rijn	2.00	4.5
OTE 1998	**32**	van Rijn	2.00	4.3
OTE 1998	**34**	van Rijn	2.00	4.5
OTE 1998	**36**	van Rijn	2.00	4.2
OTE 1998	**38**	van Rijn	2.00	4.1
OTE 1998	**40**	van Rijn	2.00	4.2

While a range of Manning's numbers are tested, only the M=30 model is described within as with the Goodwin Sands. The spatial variation in the accuracy of current speeds from the OTE models means that the results described herein to be considered in relative terms as a general trend in sediment mobility rather than an absolute quantitative measurement of volumes transported. The predicted bed level change and residual transport vectors for grain sizes of 0.16 mm and 2.00 mm are compared on a macro-scale as an initial test of whether the hydrodynamics in the region can support mobility of the two end-member grain sizes.

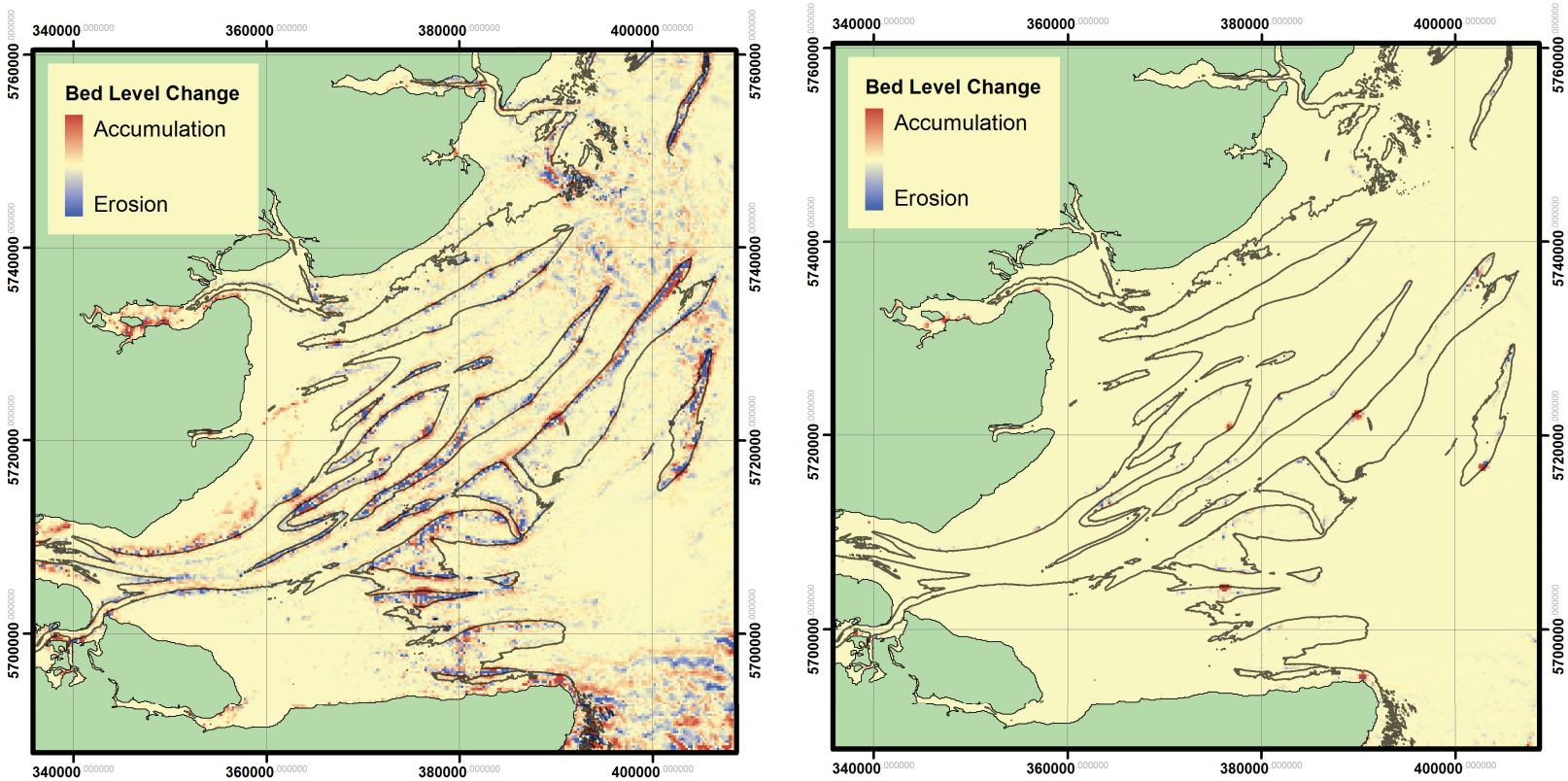

(a) Patterns of bed level change for 0.16 mm grain size in Western Zone. Accumulation and erosion appears restricted to the outer margins of the major sandbanks with a general sense of erosion along the sandbank crests.

(b) Patterns of bed level change for 2.00 mm grain size in Western Zone. Accumulation and erosion appear highly restricted to only minor regions, indicating that the hydrodynamics in the Western Zone don't support movement sediment this large.

Figure 34 – Comparison of bed level change in the Western Zone of OTE for grain sizes 0.16 mm and 2.00 mm.

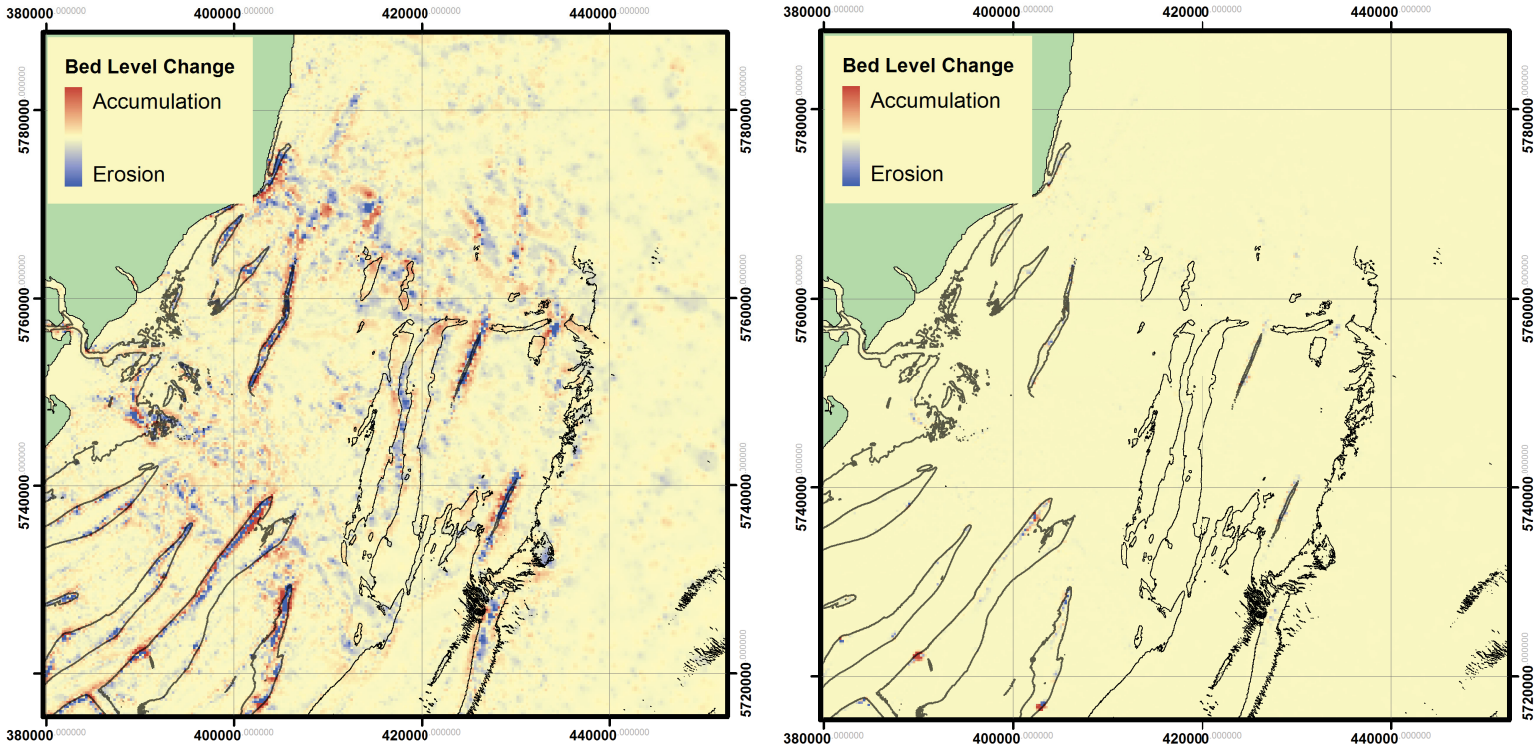

(a) Patterns of bed level change for 0.16 mm grain size in Eastern Zone. Accumulation and erosion appears to be concentrated around isolated sandbanks in the region with only minor bed level change in the majority of Eastern Zone seabed.

(b) Patterns of bed level change for 2.00 mm grain size in Eastern Zone. There is no sense of erosion or accumulation within anywhere in the Eastern Zone at this grain size, indicating that hydrodynamics don't support mobility of this sediment size.

Figure 35 – Comparison of bed level change in the Eastern Zone of OTE for grain sizes 0.16 mm and 2.00 mm.

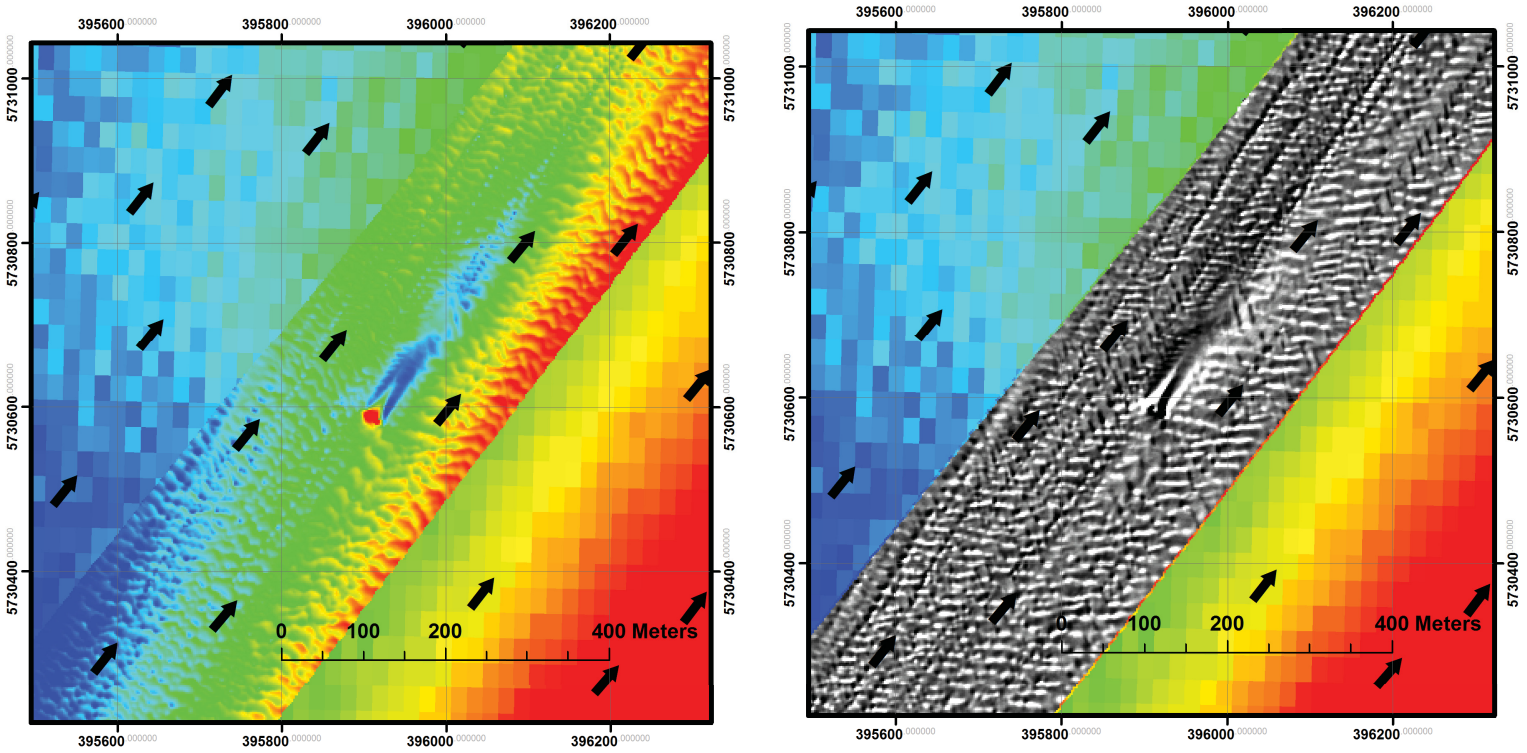

(a) Swath bathymetry showing flow-normal bedforms and symmetrical scour marks behind possible wreck.

(b) Backscatter showing flow-normal bedforms and symmetrical scour marks behind possible wreck.

Figure 36 – Comparison of high-resolution swath bathymetry and backscatter (REC, 2009) with residual transport vectors.

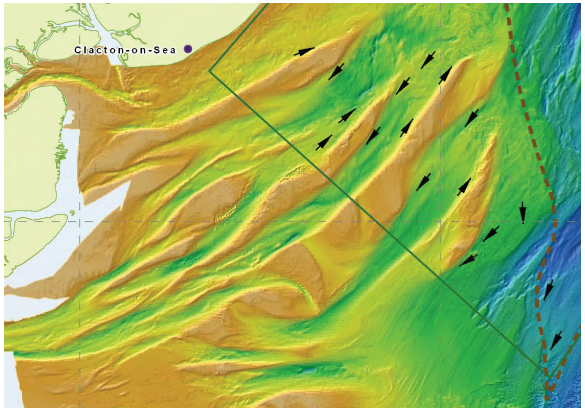

(a) Inferred sediment transport direction from backscatter and bathymetry data (REC, 2009).

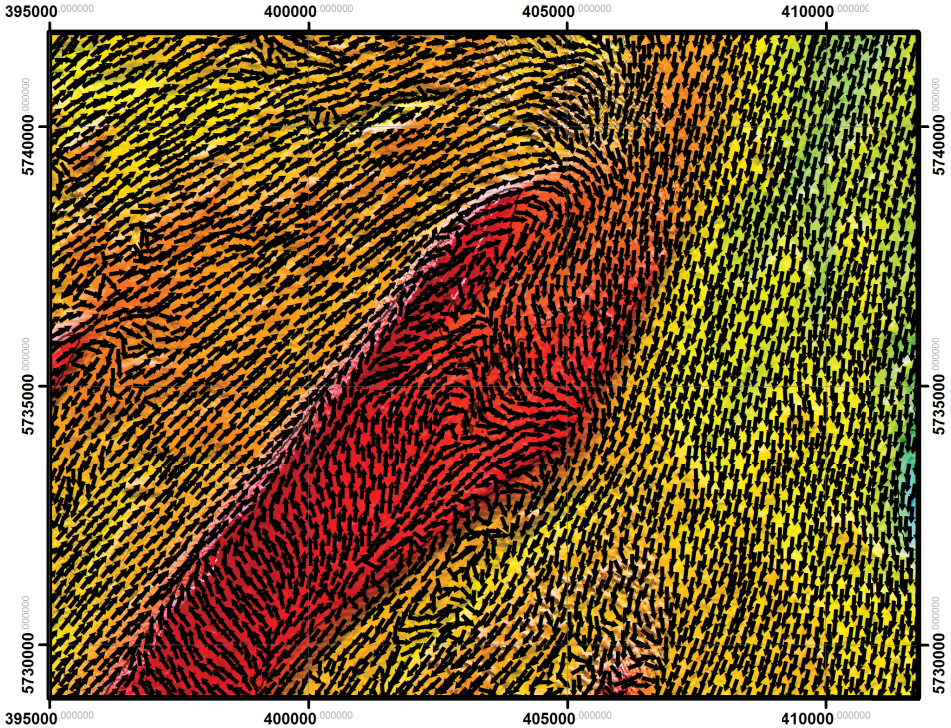

(b) Residual transport vectors at Long Sand Head, showing clock-wise movement similar to that inferred from (a).

Figure 37 – Comparison of residual transport vectors with inferred sediment transport direction from REC (2009).

4.2.1 Discussion

Previous numerical models in studying the OTE (SNS, 2002) and bathymetric analyses (Burningham & French, 2008) are the main source and comparison of sediment transport information that is available on a regional-scale in the OTE. Any physical measurements of sediment transport rates tend to be restricted to local-scale, site-specific studies for only a limited time frame. As such the sediment transport predictions obtained in this project regarded in the same aspect as those previous.

The results obtained from sediment transport predictions indicate favorable agreement between available calibration data (Fig. 36 & 37) (REC, 2009) and previous studies. A particular problem in calibration of the OTE sediment transport models is much of the available swath bathymetry and backscatter data is located along the regions where predicted flow velocity reverses direction, making interpretation difficult. However in the areas where swath data is aligned favorably, good correlation between observed bedforms and predicted flow direction was found. As discussed in Section 3, many simplications are made during the creation of the numerical model, however the good calibration results means that it is possible to draw several conclusions regarding the transport processes involved in the region.

With a uniform grain diameter of 0.16 mm, the large sandbanks in the Western Zone such as Long Sand Head show patterns of erosion and accumulation along only their margins, with no change in bed level associated in the central areas (Fig. 34). Inter-bank areas appears to be slight areas of erosion throughout the region however it must be considered that this is an artefact introduced by the use of a uniform grain size, as sample grabs (REC, 2009) show inter-bank regions to have a larger grain size (2.00 mm) similar to that of the Eastern Zone. Stronger patterns of accumulation tend to exist on north and western margins of the major banks, however no particular pattern emerges. Using a grain diameter of 2.00 mm in the transport model yields almost no bed level change throughout the Western Zone except in isolated pockets (Fig. 34). This would indicate that any patterns of erosion or deposition seen in the inter-bank regions using 0.16 mm grain size are the result of model simplification, as the model results indicate the hydrodynamics do not support mobility of larger grain sizes in the Western Zone. The trend of bathymetric deepening to the south

and shoaling to the north of the Western Zone identified by Burningham & French (2008) is not directly evident in the results presented within, with vertical accretion and erosion not appearing to be a dominant process. However, the time period studied by Burningham & French (2008) is significantly greater (c. 400 years) than that used within this project (25 days). To make a more direct comparison, it may be necessary to run a sub-sampled numerical model over a greater time period of multiple years but this would require a sacrifice in the resolution or speed at which the models are able to run.

The Eastern Zone of the OTE is primarily composed of exposed bedrock and thin sediment veneers with a mean grain size of 2.00 mm, similar to the inter-bank material found in the Western Zone. Transport modelling in this region (Fig. 35) showed no discernable change in the bed level of the zone, which would seem to indicate that active transport processes are limited to the few isolated sandbanks in the region, which show a pattern signifcant bed level change towards the smaller grain sizes. An ambient hydrodynamic regime in which the current velocities obtained are not sufficient enough to transport the dominant sediment fraction would support the hypothesis of a relict river terrace landscape as proposed by Bridgland (2004). However the proposed age of the relict landscape (c. 400-700 ka) means that for it to be preserved as is seen today any weather-related surges leading to an increase in current velocity must not be sufficient enough to mobilize the dominant sediment fraction observed in the Eastern Zone. Future work that can be undertaken to validate test this hypothesis could be to develop a hydrodynamic model that uses the currently excluded wind-, wave- and atmospheric forcing mechanisms to replicate a large storm event and determine if any sediment transport in the region occurs. One of the largest storms for which there is likely to be sufficient data to replicate the hydrodynamic conditions would be the North Sea storm of 1953 which resulted in surges of 5.6 m above MSL.

5 Conclusion

The initial development of high-resolution numerical models for predicting sediment transport within the Goodwin Sands and Outer Thames Estuary show promising results in replicating both the observed hydrodynamic regimes and net sediment transport directions for their respective regions. Calibration of the hydrodynamic models against observational hydrographic data showed that a consistently higher Manning's number was required to accurately model the observed current velocties and tidal amplitudes than dictated by physical conditions of the seabed. The degree to which the observational measurements were replicated was best in the Goodwin Sands, which because of its smaller area and single morphology type did not have accuracy reduced by generalization of the physical conditions unlike the Outer Thames Estuary.

The accuracy of predicted hydrodynamics in the Outer Thames Estuary is much more variable. The spatially-varying nature of the inaccuracies suggests that the wide range of morphology types and depths in the OTE may contribute in part to this, with the additional effects of exclusion of any fluvial inputs from the River Thames which are likely to play an important part in modelling an estuarine region. Additional work will be undertaken after completion of this project where such factors are taken into account to produced a more refined hydrodynamic regime from which to drive sediment transport models.

The resultant sediment transport predictions obtained from the calibrated hydrodynamic models are largely successful at replicating the observed net transport directions (from seabed imagery and previous studies), particularly in the Goodwin Sands where predicted bed level change appears to confirm the suggestion by Cloet (1954) that the sandbanks here undergo an anti-clockwise rotation and expansion. Similarly although the hydrodynamic model of the OTE suffers from some inaccuracies, comparison of net transport directions against bedforms observed in swath bathymetry data (REC, 2009) shows considerable agreement between the two. This is likely because although the magnitude of sediment transport is highly sensitive to the current velocity, sensitivity testing showed that the overall predicted direction reproduced the observed directions to within acceptable margins regardless of the Manning's number used. Using the predicted bed level change associated

with the two dominant sediment end-members, it was demonstrated that the ambient hydrodynamic regime in the OTE is not sufficient to drive sediment mobility of the dominant type found in the Eastern Zone. This result reinforces the hypothesis that the majority of the Eastern Zone seabed is the remains of a relict sumberged river terrace landscape (Bridgland, 2004).

This project has made significant headway into developing regional sediment mobility models for the Goodwin Sands and OTE, and identifying key steps to refine and advance the sediment transport predictions for future projects. However several obstacles at present currently limit the accuracy that can be achieved in these predictions, most notably the shortfall in the amount and type of observational measurements available to calibrate the initial outputs of the hydrodynamic models. Secondly, any increase in the resolution and time periods for which sediment transport modelling can be calculated is highly dependent upon future reductions in the cost of computing resources. Currently though, the outputs from this model can realistically be used to provide an accurate qualitative measure of patterns of accumulation and erosion and net sediment transport direction and as such is a highly useful tool for the management of underwater resources and heritage.

6 References

Anthony, E. J., 2002. Long-term marine bedload segregation, and sandy versus gravelly Holocene shorelines in the eastern English Channel. Marine Geology, 187, 221-234.

Bartlett, J. M., 1998. Quality Control Manual for Computational Estuarine Modelling, Environment Agency, R & D Technical Report W113, 80pp.

Bridgland, D. R., 1994. Quaternary of the Thames, Geological Conservation Review Series, 7, 441pp.

Burningham, H. & French, J., 2008. Historical changes in the seabed of the greater Thames estuary. The Crown Estate, 49pp.

Cazenave, P. W., 2010. Personal correspondence.

Cloet, R. L., 1954. Hydrographic analysis of the Goodwin Sands and the Brake Bank. The Geographical Journal, 120, 203-215.

Dix, J. K., Lambkin, D. O. & Cazenave, P. W., 2007. Development of a Regional Sediment Mobility Model for Submerged Archaeological Sites. English Heritage ALSF project no. 5524. SOES, University of Southampton, 156pp.

Dix, J.K., Cazenave P.W., Lambkin, D.O., Rangecroft, T., Pater, C. & Oxley, I. In: MACHU Final Report. Sediment Erosion Modelling as a tool for Underwater Cultural Heritage Management. European Union Culture 2000 Programme, Amersfoort, 2008, p 48-53.

DHI (2007), MIKE 21: Sediment Transport and Morphological Modelling - User Guide. DHI Water and Environment, Horsholme, Denmark, 388pp.

D'Olier, B., 1975. Some Aspects of Late Pleistocene-Holocene Drainage of the River Thames in the Eastern Part of the London Basin. Philosophical Transactions of the Royal Society of London. Series A, Mathematical and Physical Sciences, A Discussion on the Geology of the English Channel 279 (1288): 269-277

Dyer, K. R. & Huntley, D. A., 1999. The origin, classification and modelling of sand banks and ridges. Continental Shelf Research, 19, 1285-1330.

Emu Ltd., 2009. Outer Thames Estuary Regional Environmental Characterisation, July 2009.

Engelund, F. & Hansen, E., 1972. A Monograph on Sediment Transport in Alluvial Streams. 3rd Edition, Technical Press, Copenhagen.

Folk R. L., 1954. The distinction between grain size and mineral composition in sedimentary rock nomenclature. Journal of Geology, 62, 344-359.

HR Wallingford ,2002. Southern North Sea Sediment Transport Study, Phase 2. Sediment Transport Report EX 4526 August 2002

Kenyon, N.H., Belderson, R.H., Stride, A.H., Johnson, M.A., 1981. Offshore tidal sand banks as indicators of net sand transport and as potential deposits. Special Publication of the International Association of Sedimentologists, 5, 257-268.

Soulsby, R., 1997. Dynamics of Marine Sands. Thomas Telford, 249pp.

van Rijn, L. C., 1984. Sediment Transport: part I: bed load transport; part II: suspended load transport; part III: bed forms and alluvial roughness. Journal of the Hydraulic Division, proceedings of the ASCE, 110 (1431-56; 1613-41; 1733-53).

7 Acknowledgements

I would like to acknowledge the help of the following persons who have made the completion of this thesis possible, particularly:

My supervisor, Dr. Justin Dix, for his helpful guidance and oversight in this project and all years previous.
PhD Student Pierre Cazenave, for his continual help, advice and technical assistance.
Dr. Olivia Merritt, of the AMAP team!
All members of the SOES staff who have provided me with help and advice throughout my university career, in particular:

Dr. Tim Henstock, for his GMT skills!
Dr. Nicholas Harmon, for his MATLAB skills!
Most especially from my family and friends, including:

John Fothan
Valen Percival
Korlon Xavier
Brokin Stengah
Brennan Derrick
Mordak Shiar

Data Sources
High-resolution bathymetric dataset provided by Seazone Solutions Ltd.
Funding
I would like to thank English Heritage for funding this research project as part of the Marine Aggregate Levy Sustainibility Fund.